







Rassf7a promotes spinal cord regeneration and controls spindle orientation in neural progenitor cells

Panpan Zhu^{1,2,3,†} , Pengfei Zheng^{1,†} , Xinlong Kong⁴ , Shuo Wang¹ , Muqing Cao^{4,*}  & Chengtian Zhao^{1,2,3,*} 

Abstract

Spinal cord injury (SCI) can cause long-lasting disability in mammals due to the lack of axonal regrowth together with the inability to reinitiate spinal neurogenesis at the injury site. Deciphering the mechanisms that regulate the proliferation and differentiation of neural progenitor cells is critical for understanding spinal neurogenesis after injury. Compared with mammals, zebrafish show a remarkable capability of spinal cord regeneration. Here, we show that *Rassf7a*, a member of the Ras-association domain family, promotes spinal cord regeneration after injury. Zebrafish larvae harboring a *rassf7a* mutation show spinal cord regeneration and spinal neurogenesis defects. Live imaging shows abnormal asymmetric neurogenic divisions and spindle orientation defects in mutant neural progenitor cells. In line with this, the expression of *rassf7a* is enriched in neural progenitor cells. Subcellular analysis shows that *Rassf7a* localizes to the centrosome and is essential for cell cycle progression. Our data indicate a role for *Rassf7a* in modulating spindle orientation and the proliferation of neural progenitor cells after spinal cord injury.

Keywords asymmetric neurogenic division; *Rassf7a*; regeneration; spinal cord injury; spindle orientation

Subject Categories Cell Cycle; Neuroscience; Stem Cells & Regenerative Medicine

DOI 10.15252/embr.202254984 | Received 6 March 2022 | Revised 24 October 2022 | Accepted 27 October 2022 | Published online 21 November 2022

EMBO Reports (2023) 24: e54984

Introduction

Spinal cord injury (SCI) is one of the devastating neurological injuries and can cause long-lasting disability. Injury to the spinal cord

often results in permanent loss of motor and/or sensory function below the injured site because the sensory information ascending to the brain and the motor information descending to the body cannot go past that point (Schwab & Bartholdi, 1996; Ahuja *et al*, 2017). In mammals, the recovering abilities of the central nervous system (CNS) after injury are extremely limited, mainly due to the lack of axonal regeneration. A significant barrier to mammalian axonal regeneration during SCI is astrocyte reactive gliosis at the injury site, which invariably blocks regeneration by forming glial scars. In the central core of the lesion site, interactions between fibroblasts, inflammatory immune cells, and extracellular matrix contributes to the formation of the fibrotic scar, which is further surrounded by the astrocytes-enriched glial scars in the periphery to separate the injured area from uninjured tissues (Silver & Miller, 2004; O'Shea *et al*, 2017; Bradbury & Burnside, 2019). By contrast, spinal cord regeneration is an innate ability of axolotl (salamander) and teleost fish (zebrafish). It is supposed that these organisms may have specific mechanisms regulating glial scar formation and the following proliferation and growth process of axons (Tazaki *et al*, 2017; Ghosh & Hui, 2018).

Understanding the cellular mechanisms underlying axonal regeneration is fundamental to promote spinal cord repair after injury. Adult zebrafish have a remarkable capability of axonal regeneration following spinal cord injuries, that is, fishes can fully regenerate the spinal cord at the lesion site within 4–6 weeks (Becker *et al*, 2004; Dias *et al*, 2012). It has been suggested that the composition and response of glial cells of zebrafish are different from those of mammals, especially for the epithelial-to-mesenchymal transition (EMT) gene program (Klatt Shaw *et al*, 2021). More specifically, there is a clear absence of astrogliosis in the adult zebrafish CNS regenerating from SCI (Ghosh & Hui, 2018) and there is no permanent glial scar formation. By contrast, GFAP expressing cells elongate and form a permissive glial bridge so that the regenerating axons can actively cross the lesion

1 Institute of Evolution and Marine Biodiversity, Ocean University of China, Qingdao, China

2 Laboratory for Marine Biology and Biotechnology, Qingdao National Laboratory for Marine Science and Technology, Qingdao, China

3 Sars-Fang Centre, Ministry of Education Key Laboratory of Marine Genetics and Breeding, College of Marine Life Sciences, Ocean University of China, Qingdao, China

4 Key Laboratory of Cell Differentiation and Apoptosis of Chinese Ministry of Education, Department of Pathophysiology, Shanghai Jiao Tong University School of Medicine, Shanghai, China

*Corresponding author. Tel: +86 21 63846590 776935; E-mail: muqingcao@sjtu.edu.cn

**Corresponding author. Tel: +86 532 8203 2962; E-mail: chengtian_zhao@ouc.edu.cn

†These authors contributed equally to this work

site and reinnervate those regions caudal to injury site (Goldshmit *et al*, 2012; Mokalled *et al*, 2016). Larvae fish exhibited a faster recovery capacity after SCI than adult fish. For instance, zebrafish larvae can recover their touch-stimulate swimming behavior within two days when spinal cord injury was performed at 3 or 5 days postfertilization (dpf; Briona & Dorsky, 2014; Ohnmacht *et al*, 2016). Similar to adults, glial cells also participate in spinal cord regeneration in the larvae (Briona & Dorsky, 2014).

Multiple signaling pathways have been reported to regulate axonal regeneration after SCI in zebrafish. For example, Wnt/ β -catenin signals are activated in spinal radial glia cells after SCI, and overexpression of Dkk1b, a negative regulator of Wnt signaling, prevents glial bridge formation, as well as axonal regeneration (Briona *et al*, 2015; Strand *et al*, 2016). Interestingly, inhibition of Wnt signaling specifically in the glial cells does not impair axonal regeneration, suggesting that Wnt/ β -catenin signals may regulate axonal regeneration via nonglial cells. Indeed, the fibroblast-like cells accumulated in the lesion site are able to express and deposit Collagen XII upon Wnt signaling activation, which is essential for axonal regeneration and functional recovery after SCI (Wehner *et al*, 2017). A recent study showed that the extracellular matrix components were partially regulated by a specific type of Pdgfr⁺ cells recruited to the lesion site (Tsata *et al*, 2021). FGF signals are also critical for axonal regeneration. After SCI, glial cells proliferate and change their morphology to form the glial bridge in favor of axonal regeneration as a response to these signals (Goldshmit *et al*, 2012). Of note, different Fgfs play distinct roles in regulating neurogenesis after SCI, with Fgf2 and Fgf8 being more effective in facilitating neurite outgrowth (Goldshmit *et al*, 2018). Similarly, activated FGF2 signaling also promotes axonal regeneration after SCI in mice and humans (Goldshmit *et al*, 2014; Ko *et al*, 2018).

In anamniotes, newborn neurons are generated rapidly after SCI to promote axonal regeneration as well as developing other cell types of neurons that are essential for recovering a fully functional spinal cord. These newly formed neurons are mainly differentiated from a specific type of neural progenitor cells, an astroglia-like radial glia localized to the central canal (Becker & Becker, 2015; Becker *et al*, 2018). These radial glial cells form part of the ependymal layer and have radial processes extending from the central canal toward the pial surface. Several stem cell markers, including Sox2 and Pou5f1, are expressed in these progenitor cells, which are essential for neurogenesis after SCI (Fei *et al*, 2014; Ogai *et al*, 2014; Hui *et al*, 2015). During neurogenesis, radial glia cells can either divide symmetrically to expand the pool of neural precursors or undergo an asymmetric neurogenic division that produces another radial glia and a newborn neuron (Becker & Becker, 2015; Shohayeb *et al*, 2021). During symmetric proliferative division, the cleavage plane is usually perpendicular to the apical membrane resulting in equal distribution of proteins between daughters. The cleavage plane is prone to be horizontal or oblique when the radial glia undergoes an asymmetric division, in which neurons are mostly generated from the more apical daughter cell (Konno *et al*, 2008; Alexandre *et al*, 2010; Postiglione *et al*, 2011; Shao *et al*, 2020). Asymmetric division of radial glia cell is also observed in adult zebrafish after spinal cord injury (Reimer *et al*, 2008; Hui *et al*, 2010).

The Ras-association domain family (RASSF) proteins contain 10 members, all of which are characterized by the presence of a Ras-

association (RA) domain. Depending on the position of the RA domain, RASSF proteins can be classified as C-terminal (classical) RASSFs (RASSF1-6) or N-terminal RASSFs (RASSF7-10). The RA domain interacts with the RAS GTPase family of proteins to regulate many cellular processes, including membrane trafficking, apoptosis and proliferation (Kitagawa *et al*, 2006; Richter *et al*, 2009; Underhill-Day *et al*, 2011). The classical RASSF family members are generally considered as tumor suppressors and have been reported to participate in many biological processes, such as microtubule stability, cell cycle control and apoptosis, whereas N-RASSF proteins, which have been less studied, seem to play diverse roles during cell growth, apoptosis and embryonic development (Underhill-Day *et al*, 2011). RASSF7 has been suggested to play a role during mitosis through regulating microtubule dynamics (Sherwood *et al*, 2008; Recino *et al*, 2010; Gulsen *et al*, 2016). RASSF7 can promote cell proliferation through MEK1/2-ERK1/2 signaling pathway activation (Wang *et al*, 2016; Zhang *et al*, 2018a). *In vitro* studies have also showed that, through interaction with N-RAS, RASSF7 inhibits mitogen-activated protein kinase kinase (MKK) 7 phosphorylation to negatively regulate pro-apoptotic JNK signaling under stress-induced conditions (Takahashi *et al*, 2011).

Here, we reported the role of *Rassf7* during spinal cord regeneration in zebrafish. Zebrafish *rassf7a* mutants displayed significant regeneration defects after spinal cord injury, which were mainly due to the restricted cell proliferation of the neural progenitor cells. We further provided data to show that *rassf7a* encodes a centrosomal protein and regulates spindle orientation during radial glia proliferation. These results suggested an important role of *Rassf7a* in spinal cord regeneration of zebrafish larvae after injury, which may help us to understand the reasons for the failure of axonal regeneration in mammals.

Results

Tissue-specific expression of *rassf7a* and *rassf7b* during early embryogenesis

When searching for cilia-related genes via whole-mount *in situ* hybridization assay, we identified two *rassf7* homologous genes, *rassf7a* and *rassf7b*, in zebrafish. Zygotic *rassf7a* was first detected in the dorsal forerunner cells (DFCs), at around 90% epiboly stage (Appendix Fig S1A). At 14-somite stage, *rassf7a* expression was initially enriched in the third and fifth rhombomeres, as suggested by double *in situ* staining with *krox20*, a well-known hindbrain marker (Appendix Fig S1B). At 18-somite stage, *rassf7a* started to be expressed in the neural tube, and showed abundant expression in the whole central nervous systems at 24 h postfertilization (hpf; Fig 1A, Appendix Fig S1C). Transverse sections through the trunk suggested that *rassf7a* was expressed in the whole neural tube with high enrichment in the central canal at both 24 and 72 hpf (Fig 1B and C). Similarly, *rassf7b* was also expressed in the DFCs, starting at 75% epiboly stage (Appendix Fig S1D). At 10-somite stage, expression of *rassf7b* was observed mainly in the Kupffer's vesicle (KV; Appendix Fig S1E). At 24 hpf, *rassf7b* expression was selectively enriched in the pronephric duct, olfactory placode, otic vesicle and posterior notochord (Appendix Fig S1F).

Generation of *rassf7* zebrafish mutants

The expression pattern of *rassf7b* is similar to those of genes involved in cilia development (Song *et al*, 2016; Han *et al*, 2018; Zhang *et al*, 2018b), promoting us to first investigate the role of Rassf7b during ciliogenesis. We generated zebrafish *rassf7b* mutants using the TALEN system and identified a mutant line carrying a 7-bp

deletion in the target site (Appendix Fig S2A). We further confirmed this deletion through Sanger sequencing of the mutant transcripts, which suggested that this deletion caused a frameshift during messenger RNA (mRNA) translation, resulting in the disruption of the Ras-association domain of Rassf7b protein (Appendix Fig S2A and B). The expression level of the mutant transcripts was also decreased due to nonsense-mediated decay (Appendix Fig S2C and D).

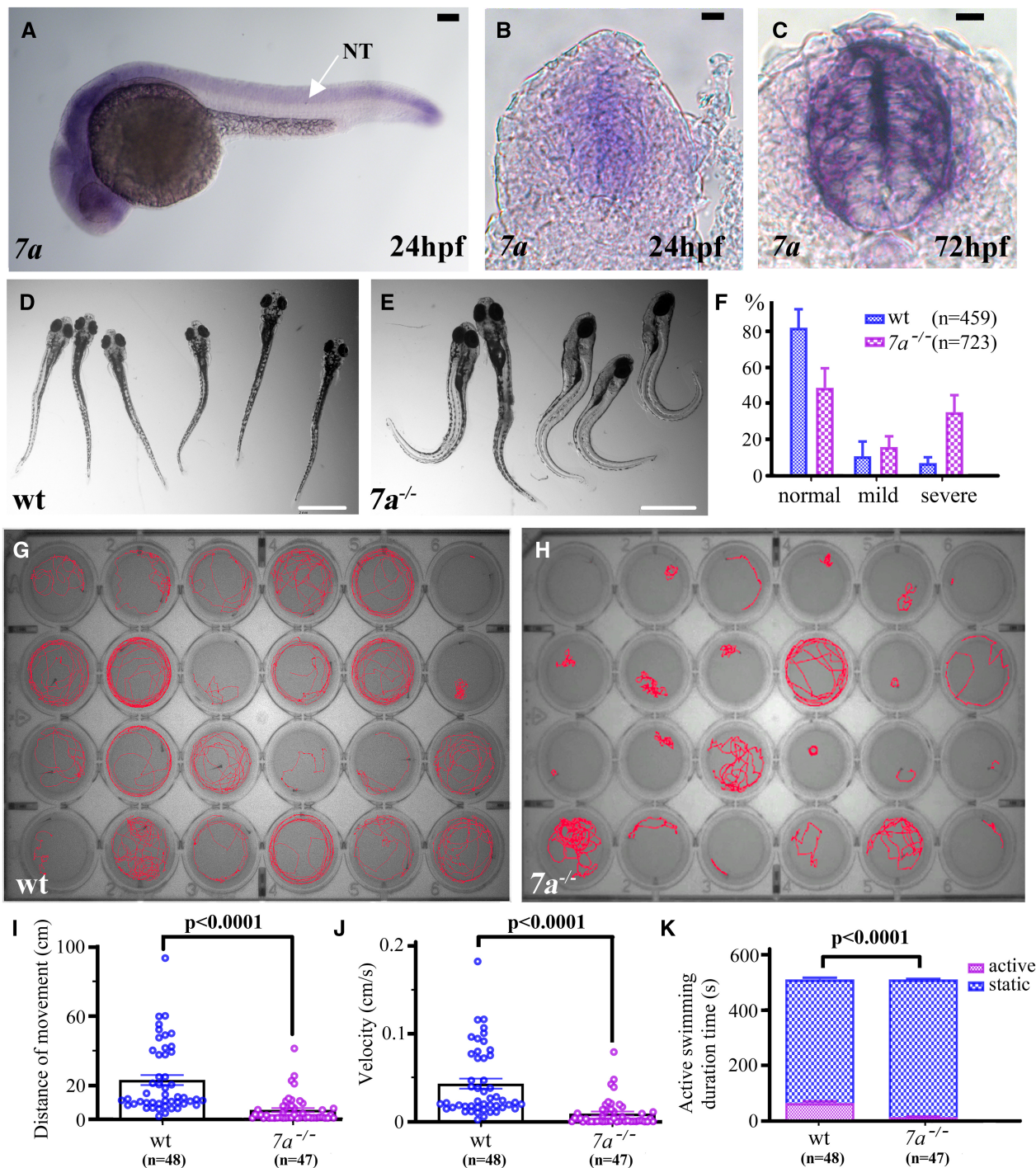


Figure 1.

Figure 1. Locomotion defects of *rassf7a* mutants after SCI.

- A Whole mount *in situ* hybridization results showing expression of *rassf7a* at 24 hpf.
 B, C Cross sections through the trunk region showing the expression of *rassf7a* in the spinal cord of 24 and 72 hpf zebrafish larvae.
 D, E External phenotypes of wild-type (D) and *rassf7a* mutant (E) larvae at 6 dpi.
 F Bar graph showing the percentages of larvae with normal, mild and severe body axis defects in wild-type ($n = 459$) or *rassf7a* mutants ($n = 723$) at 6 dpi.
 G, H Locomotion tracking of each individual larva of wild-type (G) or *rassf7a* mutants (H) at 6 dpi in 24-well plates.
 I Dot plots showing the swimming distance of each larva at a duration of 500 s.
 J Dot plots showing the swimming velocity of wild-type and mutant larvae as indicated.
 K Bar graph showing active swimming time in wild-type and mutant larvae at a duration of 500 s.

Data information: In panels I and J, each dot represents an individual larva. *P* values for unpaired Mann–Whitney test (I, J) and Two-way ANOVA with Bonferroni's multiple comparisons test (K) are indicated. Data are shown as mean \pm S.E.M. Scale bars: 100 μ m in (A–C) and 1 mm in (D and E).

Surprisingly, zebrafish *rassf7b* mutants were viable and fertile. Whole-mount immunohistochemistry with an anti-acetylated tubulin antibody suggested that cilia were grossly normal in *rassf7b* mutants (Appendix Fig S2E–I).

Considering that *Rassf7a* may play a redundant role in *rassf7b* mutants, we further generated *rassf7a* mutants carrying a 4-bp deletion in the target area (Appendix Fig S2A and B). The expression level of mutant mRNA was also substantially decreased in the mutants (Appendix Fig S2C and D). We further generated *rassf7a*; *rassf7b* double mutants ($7a^{-/-};7b^{-/-}$). Strikingly, double homozygous mutants were also viable and fertile. Of a total of 263 adults crossed from double heterozygote mutants, we identified 15 double homozygous mutants, including seven females and eight males, which suggest that *Rassf7* proteins are dispensable for the growth of zebrafish. In addition, cilia were also grossly normal in the double mutants (Appendix Fig S2E–I). Being derived from DFCs, Kupffer's vesicle is an essential organ for the establishment of left–right asymmetry (Essner *et al*, 2005). Although both *rassf7* genes were expressed at a high level in the DFCs, there were no laterality defects in the double mutants, as indicated by the expression of *lefty-2*, an asymmetry marker expressed in the lateral plate mesoderm of early zebrafish larvae (Appendix Fig S2J; Zhao & Malicki, 2007). Moreover, the number and length of cilia in the Kupffer's vesicle was comparable between control and mutant embryos (Appendix Fig S2E–G). These data suggested that *Rassf7* proteins were neither essential for ciliary development, nor for left–right asymmetry determination.

Locomotion defects of *rassf7a* mutants after SCI

Although *rassf7a* showed abundant expression in the central nervous systems, the development of spinal cords was grossly normal in *rassf7a* mutants as suggested by the normal thickness visualized via Tg(*huc:GFP*) or Tg(*foxj1a:HA-tdTomato*) transgenic lines (Appendix Fig S3A–E). We further asked whether mutant spinal cord will exhibit developmental defects in stress-induced conditions. Considering the high expression of *rassf7a* in the central nervous systems (Fig 1A–C), we evaluated the regeneration efficiency of spinal cord after injury. For this, we transected the spinal cord with a beveled microinjection pipette at 3 days post-fertilization and investigated the regeneration efficiency at different time points after injury (Fig EV1A and B). Similar to previously report, the wound sites were gradually closed at around 48 h post-injury (hpi; Ohnmacht *et al*, 2016). Spinal cord was fully regenerated at around 7 days after transection

(Fig EV1C). After regeneration, most larvae displayed a straight body axis, while some exhibited dorsal bending at varying degrees (Fig EV1D). Surprisingly, we found a significant increase in the percentage of embryos exhibiting dorsal bending phenotype in *rassf7a* mutants after SCI (16% in wild-type, $n = 459$ vs 60% in the mutants, $n = 723$; Fig 1D–F). In most cases, regenerated larvae with severe dorsal bending failed to swim straight and could not react properly to touch stimulus (Movies EV1 and EV2).

To further analyze locomotion, we monitored the behavior of zebrafish larvae at 6 days post-injury (dpi) using EthoVision XT11, a professional behavior tracking software (Fig 1G and H). Under the tapping stimulus condition, the motion distance and velocity decreased significantly in the mutant larvae (Fig 1G–J). Moreover, mutant larvae static state lasted longer than that of control zebrafish (Fig 1K). We further compared the motion capability of wild-type and mutant larvae with straight and curved body axis at 6 dpi. Clearly, the movement of larvae with dorsal bending was significantly weaker than those of the straight larvae in both wild-type and mutant groups (Fig EV1E and F). Strikingly, wild-type larvae with straight body axis were also more active than those of mutant larvae with straight body axis (Fig EV1G). These data suggested that *rassf7a* mutant embryos exhibited locomotion defects at 6 days after spinal cord injury.

Axonal regeneration defects in *rassf7a* mutants after SCI

To clarify the reason of locomotion defects in mutants, we generated *rassf7a* homozygous mutants carrying either the Tg(*gfap:GFP*) or Tg(*huc:GFP*) transgene, which labels neural glial and neuronal cells respectively. These transgenes allow for the gap in the lesion sites to be easily visualized after injury (Fig 2A). In wild-type larvae, both HuC and GFAP expressing cells started to accumulate at the injury site rather quickly between 1 and 3 days after injury (Fig 2A–C). Till 7 dpi, the fluorescence gaps were almost completely recovered for both wild-type transgenes (Fig 2A). Interestingly, we found no difference in the areas of GFP expression in the glial cells at the lesion sites between wild-type and *rassf7a* mutants (Fig 2B). By contrast, the recovery of fluorescence signals in the Tg(*huc:GFP*) transgene were significantly delayed in the mutants (Fig 2C). We further measured the thickness of GFP fluorescence signals in both straight and curved larvae at 5 and 7 dpi. As shown in Fig EV1, the regenerated HuC⁺ fascicles were significantly thinner in both straight and curved larvae of the mutants (Fig EV1H–J).

We further employed *rassf7a*-targeted vivo morpholinos (MOs) to knockdown *rassf7a* expression in wild-type embryos. The

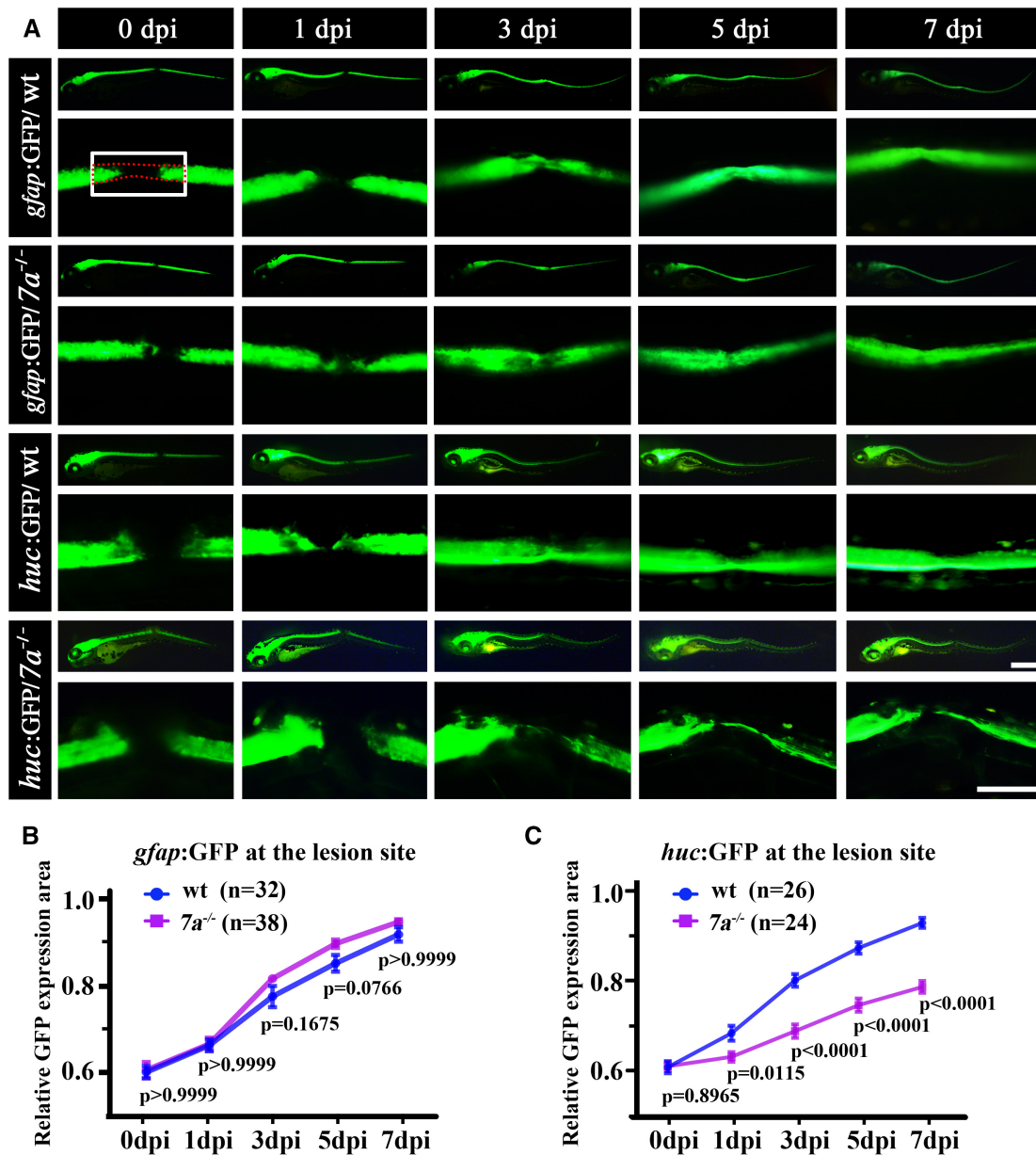


Figure 2. Recovery of neural and glial cells in *rassf7a* mutants after injury.

A Representative images showing GFP expression in wild-type or *rassf7a* mutants carrying Tg(*gfap:GFP*) or Tg(*huc:GFP*) transgene at different time points as indicated. Bottom rows showing the magnified views near the lesion sites.

B Line plots showing relative expression level of GFP fluorescence at the lesion sites in wild-type and *rassf7a* mutants at different time points as indicated.

C Statistical results showing relative expression area of GFP fluorescence at the lesion sites of Tg(*huc:GFP*) transgenic larvae.

Data information: In panel (A), the white rectangle and red dashed box indicate the fixed size for GFP fluorescence measurement and the neural tube respectively.

Relative GFP expression area was calculated by the ratio of the GFP expression area in the white rectangle to the size of the neural tube (see methods for the details). *P* values for Two-way ANOVA with Bonferroni's multiple comparisons test (B, C) are indicated. Data are shown as mean \pm S.E.M. *N* = 7 biological replicates per group. Each data point represents an average of each group as indicated. Scale bars: 500 μ m.

knockdown efficiency of this MO was first validated via coinjection with a reporter construct at one cell stage, which showed that this MO can reduce the expression of GFP to the background level (Appendix Fig S4A–C). Next, we injected *rassf7a* or control MOs into the Tg(*huc:GFP*) transgenic embryos at the lesion sites

immediately after injury and found that *rassf7a* knockdown significantly obstructed the recovery of GFP fluorescence (Appendix Fig S4D and E). Meanwhile, we overexpressed Rassf7a protein in the mutants by injecting *rassf7a* under a heat shock inducible promoter. After heat shock, the GFP fluorescence signals

improved significantly, while overexpression of tdTomato alone failed to prevent the regeneration defects in the mutants (Appendix Fig S4F). Of note, ectopic expression of *Rassf7a* also slightly increased the recovery of GFP fluorescence in wild-type larvae (Appendix Fig S4G).

Axonal regrowth is necessary for the functional recovery of spinal cord in larval zebrafish (Bhatt *et al*, 2004; Ohnmacht *et al*, 2016), we further analyzed axonal regrowth and glial bridge formation in the mutants through a combination of immunohistochemical (anti-acetylated alpha tubulin staining) and transgenic marker (*gfap:GFP*) labeling. Similar to previous report (Wehner *et al*, 2017), the majority of fascicles (65%, $n = 58$ fascicles) that entered the lesion sites were composed of axonal-only processes at 1 dpi in wild-type larvae (Fig EV2A and B). The glial-only and mixed processes were also detectable (Fig EV2B). Noticeably, the proportion of these fascicles were similar between mutant and control larvae (Fig EV2A and B). The percentages of larvae with axonal or glial processes were comparable, and the axonal bridges were also of similar length between mutant and control larvae at 1 dpi (Fig EV2C and D). By contrast, the thickness of these axonal bundles was significantly reduced in both straight and curved groups of the mutant larvae at 5 dpi (Fig EV2E and F). These data revealed that the initial formation of axonal and glial bridge was not affected, while axonal regeneration during later stages were inhibited in the absence of *Rassf7a*.

Mutation of *Rassf7a* affected the neuronal differentiation of newborn cells

The later-onset axonal regeneration defects in the mutants may due to the deficiencies of the production of neuronal cells at the lesion sites. To test this, we evaluated the numbers of newborn neurons via BrdU labeling. Starting at 1 day after injury, multiple BrdU⁺ cells accumulated at the lesion sites (Fig 3A). These BrdU⁺ cells include differentiated neuronal cells (*huc:GFP*), glial cells (*gfap:GFP*), together with cells involved in immune response and dermal and myogenic repair as previously reported (Suzuki *et al*, 2005). Noticeably, we observed a higher number of BrdU⁺ neurons or glial cells in the wounded region at 3 dpi, while the number of these BrdU⁺ cells decreased at 5 dpi with the recovery of spinal cord (Figs 3A–F and EV3). Next, we compared the number of BrdU⁺ neurons between wild-type and mutant larvae. As shown in Fig 3, the number of BrdU⁺ neurons decreased significantly in *rassf7a* mutants (Fig 3B–E). By contrast, there was no significant difference in the number of BrdU⁺ glial cells between wild-type and mutant larvae (Fig 3B–D and F). These results implied that *Rassf7a* loss mainly affected the neuronal differentiation of newborn cells.

During neurogenesis in zebrafish larvae, neurons are mainly differentiated from neural progenitor cells (NPCs). The reduced number of BrdU⁺ neuronal cells promoted us to further investigate whether *Rassf7a* malfunction can cause proliferation defects of the neural progenitors. Sox2 is one of the earliest transcription factors expressed in neural stem and progenitor cells (Graham *et al*, 2003). We further analyzed the proliferating ability of Sox2 expressing cells after spinal cord injury by co-immunostaining anti-Sox2 antibody with antiproliferating cell nuclear antigen (PCNA) antibody, a marker of cell proliferation (Fig 3G). In the spinal cord, Sox2 is

mainly expressed in the radial glial progenitor cells near the central canal. High number of proliferating cells (Sox2⁺/PCNA⁺) can be easily identified at the lesion sites in wild-type larvae (Fig 3G–I). By contrast, the number of Sox2⁺/PCNA⁺ cells was significantly decreased in *rassf7a* mutants (Fig 3G–I). Altogether, these data suggested that *Rassf7a* regulates the proliferation of neural progenitor cells and the neuronal differentiation of newborn cells after SCI.

rassf7a is mainly expressed in neural progenitor cells

The proliferation defects of neural progenitors suggested that *Rassf7a* may regulate the differentiation of these cells directly. Next, we asked whether *rassf7a* was expressed in these progenitor cells. First, we performed fluorescence *in situ* hybridization (FISH) to check the colocalization between *rassf7a* and several markers of different neural cell types, including neuronal cells (*huc*) and neural progenitors (*msi1* and *sox2*). At 24 hpf, *rassf7a* expression was distributed throughout the neural tube (Fig 1A–C, Appendix Fig S5). While we did not find colocalization between *rassf7a* and *huc*, part of *rassf7a* was colocalized with *msi1* and *sox2* expression (Appendix Fig S5A–I). Noticeably, both *msi1* and *sox2* were widely expressed in the neural tube at this stage, suggesting a broad distribution of neural progenitors at early stages (Appendix Fig S5E and H). The expression level of *rassf7a* decreased substantially in the mutants, further confirmed the specificity of these fluorescent signals as well as NMD effects of the mutants (Appendix Fig S5A'–I'). At 3 dpf, the expression of *rassf7a* was mainly accumulated in the central canal, where the neural progenitor cells were dispersed as indicated by *sox2* and *msi1* staining. We detected strong overlap signals between *rassf7a* and *msi1*, *sox2* near the central canals, where the staining of *huc* was absent (Fig 4A–O).

Next, we performed fluorescence-activated cell sorting (FACS) experiment to confirm the co-location between *rassf7a* and *sox2*. First, we sorted Huc⁺ cells and Sox2⁺ cells from Tg(*huc:GFP*) or Tg(*sox2:sox2-2a-sfGFP*) transgenic larvae at 3 dpf. Quantitative real-time PCR (qPCR) results showed that *rassf7a* was mainly present in the Sox2⁺ cells with lower detectable levels in Huc⁺ cells (Fig 4P). In addition, the expression level of *rassf7a* in the Sox2⁺ cells was comparable between control (uninjured) and injured larvae at 10 hpi, while the expression of *rassf7a* increased significantly at 3 days after injury (Fig 4Q and R). Furthermore, we plotted the *rassf7a*-expressing cells from two published single-cell transcriptomes (Cavone *et al*, 2021; Scott *et al*, 2021). The expression of *rassf7a* is mainly enriched in those neural progenitor clusters expressing GFAP and Sox2 (Fig EV4A–D). Altogether, these data suggested that the expression of *rassf7a* was highly enriched in the neural progenitor cells at larvae stage.

Rassf7a regulates mitotic spindle orientation in NPCs

We next sought to characterize the cellular basis of cell proliferation defects in NPCs by performing time-lapse analysis using a Tg(*sox2:sox2-2a-sfGFP*) knock-in transgenic line (Shin *et al*, 2014). In wild-type larvae, the dividing GFP⁺ NPCs can be detected near the lesion sites. Noticeably, we observed slightly rotation of the longer dividing axis during metaphase to anaphase transition (Movie EV3, Fig 5A and B), reminiscent of the mitotic-spindle rotations occurred in a variety of controlled cell divisions (Kaltschmidt *et al*, 2000;

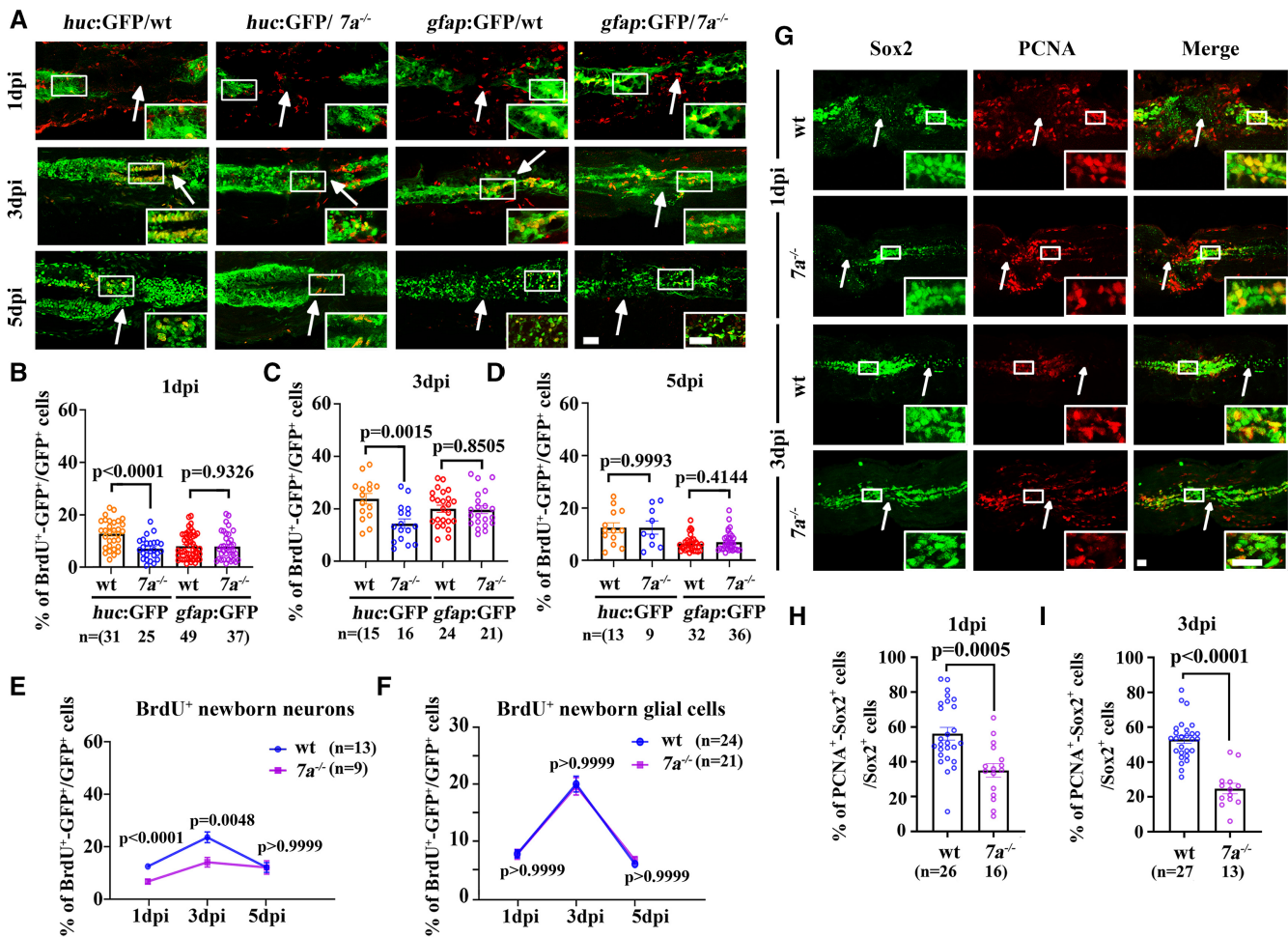


Figure 3. Neuronal differentiation defects in *rassf7a* mutants after SCI.

A Confocal images showing localization of BrdU positive cells (red) near the lesion sites in wild-type and *rassf7a* mutants carrying different transgenes. Inserted images are magnified views.

B–D Dot plots showing the percentages of BrdU/GFP double labeled cells in wild-type and *rassf7a* mutants at different time points as indicated.

E Statistical plot showing percentages of BrdU labeling neuronal cells at different time points.

F Statistical plot showing percentages of BrdU labeling neural glia cells at different time points after SCI.

G Confocal images showing proliferating neural progenitor cells visualized with anti-Sox2 (green) and anti-PCNA (red) antibodies in wild-type and *rassf7a* mutants after SCI.

H, I Dot graphs showing percentages of proliferating Sox2 positive cells in wild-type and *rassf7a* mutants at one day (H) and three days (I) after spinal cord injury.

Data information: Arrows in (A, G) represent lesion sites. Individual channels of panel (A) were shown in Fig EV3. *P* values for unpaired Student's *t*-test (*huc:GFP* group in B and D, C, H, I), unpaired Mann–Whitney test (*gfap:GFP* group in B and D) and two-way ANOVA with Bonferroni's multiple comparisons test (E, F) are indicated. Data are shown as mean ± S.E.M. *N* = 3–5 biological replicates per group in (A–F), *N* = 3 biological replicates per group in (G–I). Each data point represents an individual fish in (B–D) and (H and I), and averages of each group were indicated in (E, F). Scale bars: 20 μm in (A, G).

Haydar *et al*, 2003; Fededa *et al*, 2016). We measured the rotation angles of the spindle axes between their initial position at the metaphase and final dividing position at the anaphase (Fig 5B). In wild-type larvae, the spindle rotation of these NPCs was mainly restricted to a small field, ranging from 0° to 45° (average = 31.07° ± 5.446°, mean ± S.E.M.; Fig 5C). By contrast, cell divisions were relatively less common in *rassf7a* mutants. The spindle rotation angles were significantly increased to a great extent in the mutants with an average of 55.76° ± 8.989° (mean ± S.E.M.; Fig 5C–E, Movie EV4). Such abnormal mitotic spindle rotation of NPCs was also present in

the *rassf7a* morphants (Fig EV5A–D). In some case, we could see cell rotates nearly 360° (Movie EV5). Moreover, the rotation defects also delayed the mitosis process as demonstrated by the elongated cell division time (Figs 5F and EV5E).

Cell divisions of the NPCs can be either symmetric or asymmetric. The symmetric division expands the pool of progenitor cells, while asymmetric division produces another daughter progenitor cell and, most importantly, a second daughter cell that can be further differentiated into neurons (Alexandre *et al*, 2010). The generation of symmetric or asymmetric cell division is mainly regulated

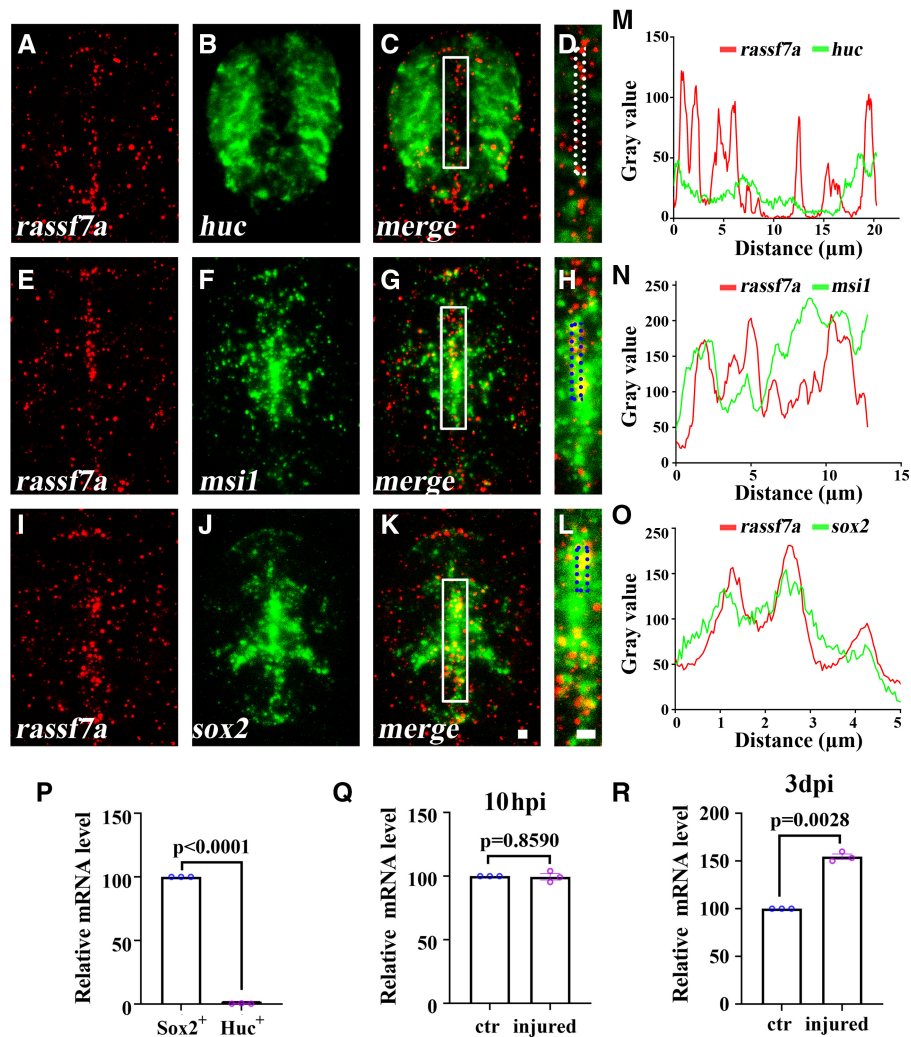


Figure 4. Expression of *rassf7a* is enriched in Sox2⁺ neural progenitor cells.

A–L Double fluorescence *in situ* hybridization results showing the localization of *rassf7a* (A, E, I) and *huc* (B), *msi1* (F) or *sox2* (J) on the cross sections of spinal cord of 72 hpf zebrafish larvae. Panels (D), (H) and (L) are magnified views of the boxes indicated in panels (C), (G) and (K).

M–O Line profile plots showing the pixel intensities of green and red channels along the dotted rectangles as indicated in panels (D), (H) and (L).

P qRT-PCR results showing the relative expression level of *rassf7a* in Sox2⁺ or Huc⁺ cells as indicated.

Q, R qRT-PCR results showing the relative expression level of *rassf7a* in Sox2⁺ cells between control and injured larvae at 10 hpi (Q) and 3 dpi (R) as indicated.

Data information: *P* values for unpaired Student's *t*-test with Welch's correction (P–R) are indicated. Data are shown as mean \pm S.E.M. *N* = 10–12 biological replicates per group in (A–L). *N* = 3 biological replicates per group in (P–R). Each data point in (P–R) represents a biological replicate. Scale bars: 10 μ m in (A–L).

by spindle orientation of the NPCs. During neurogenesis, several studies have showed that neurons are prone to be generated from the more apical daughter cells during the asymmetric perpendicular division (the cleavage plane is close to parallel to the apical surface; Bultje *et al*, 2009; Alexandre *et al*, 2010; Dong *et al*, 2012). Similarly, by microinjecting *H2B-GFP* mRNA into the Tg(*huc:Gal4;uas-mCherry*) double transgenic embryos, we observed the expression of mCherry in the daughter cells from three out of eight cells undergoing perpendicular division (Movie EV6). In one case, we also found that mCherry proteins are expressed in both daughter cells differentiated from a vertically divided cell (Movie EV7). By contrast, we did not find any red fluorescence signals in the daughter

cells from planar symmetric division of the NPCs ($n = 8$; Movie EV8). These data suggested that perpendicular division of NPCs is critical for the generation of neurons.

Next, we further explored the final orientation of cell divisions by measuring the angles between cell division axis and the anterior–posterior axis (Fig 6A and B). In wild-type larvae, more than 50% of the progenitor divisions were within 45° of the dorsal–ventral axis with the maximum occurring in the 75–90° sector, which probably would undergo an asymmetric division to generate differentiating neurons (Fig 6B and C). In *rassf7a* mutants, over 63% of cell divisions were within 30° of the anterior–posterior axis with the maximum occurring in the 0–15° sector, which were prone to undergo

planar division and generate two daughter progenitor cells (Fig 6C). These results were further confirmed via *rassf7a* morpholino (Fig 6A and D). Together, these time-lapse results showed that both cell proliferation and spindle orientation of the proliferating NPCs were affected in the absence of *Rassf7a*.

RASSF7 is essential for mitosis in cultured cells

The proliferation defects of the NPCs in the mutants suggested a role of *Rassf7* during cell division, which promoted us to further characterize the subcellular localization profile of *Rassf7* during mitosis.

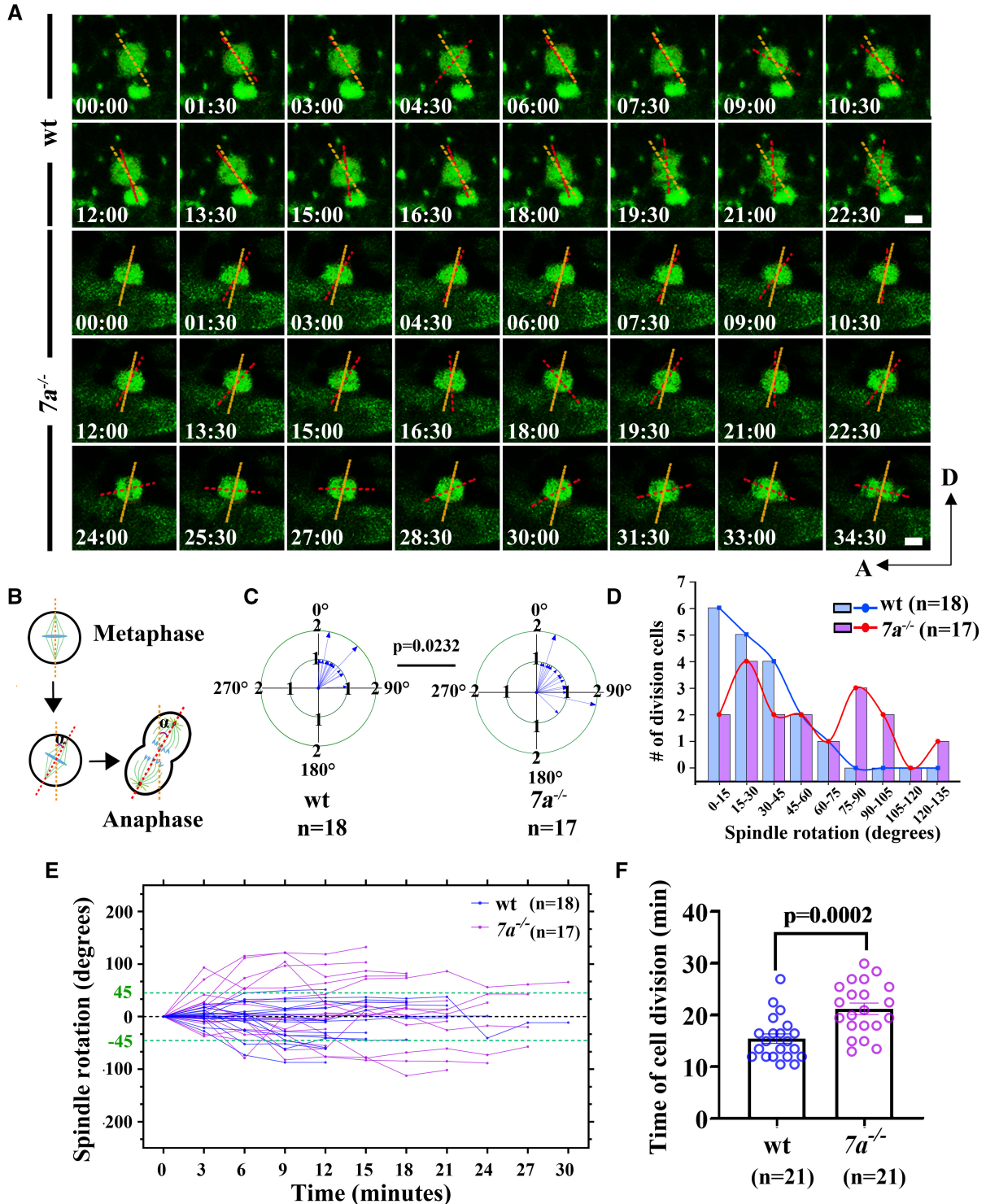
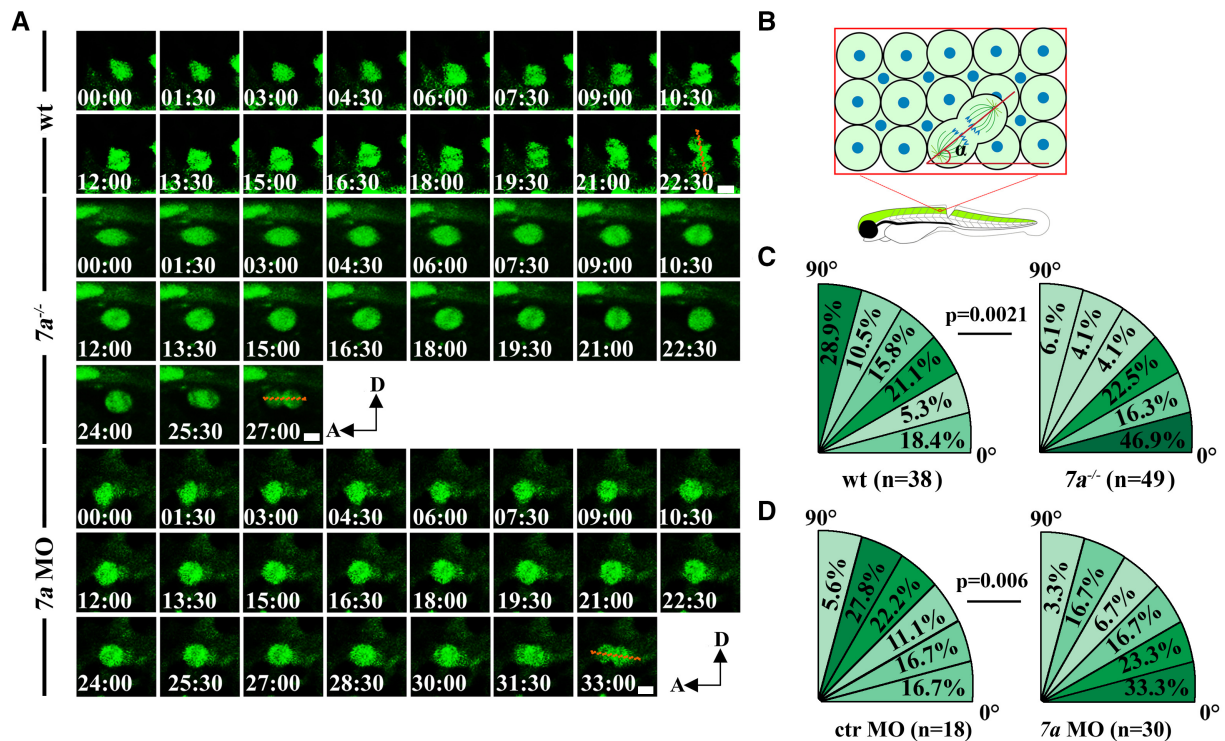


Figure 5.

Figure 5. Abnormal mitotic spindle rotation of NPCs in *rassf7a* mutants after SCL.

- A Sequences of time-lapse photographs to illustrate mitotic rotation of a single neural progenitor cell in wild-type or *rassf7a* mutants expressing Sox2⁺-GFP transgene. Anterior is to the left, dorsal is to the up. Time is in min:sec.
- B Diagram showing the rotation angles of the spindle axis during metaphase (orange dashed line) to anaphase (red dashed line) transition.
- C Statistical analysis of angles of mitotic spindle rotation in wild-type or *rassf7a* mutants. The outer circle indicates the same rotation angles occurred in two individual cells. The number of NPCs counted is shown in the bottom.
- D Statistical plot showing the distribution of dividing cells with different rotation angles in wild-type and *rassf7a* mutants.
- E History plots of mitotic spindle orientation in wild-type and *rassf7a* mutants at different time points. Green dashed lines indicate 45° spindle rotation.
- F Bar graph showing the time of NPCs division in wild-type and *rassf7a* mutants.

Data information: *P* values for unpaired Student's *t*-test (C) and Mann–Whitney test (F) are indicated. Data are shown as mean ± S.E.M. Each data point represents a cell. Scale bars: 5 μm.

**Figure 6. Spindle orientation defects in *rassf7a* mutants.**

- A Time-lapse images showing representative NPCs undergoing perpendicular (wt) or horizontal (mutant and morphant) cell division. The red dashed lines indicate spindle orientation at anaphase.
- B Diagram illustrating how the spindle angle was measured between axes defined by the anaphase spindle and anterior–posterior.
- C Distribution of dividing NPCs with different spindle angles in wild-type and *rassf7a* mutants.
- D Spindle orientation in control and *rassf7a* morphants. The percentages of progenitor cells with different spindle angles are shown within six 15° sectors. *n* represents the number of NPCs. Time is in min:sec. Anterior is to the left, dorsal is to the up.

Data information: *P* values for Fisher's exact test (C, D) are indicated. Scale bars: 5 μm.

First, we generated stable cell line expressing Flag-tagged RASSF7 in hTERT-RPE-1 cells and determined the protein localization during mitosis using anti-Flag antibody. Immunofluorescence showed that RASSF7 localized to the cytoplasm with enrichment in the centrosome during interphase, as demonstrated by the colocalization analysis with γ -tubulin and PCM1, two centrosomal markers (Fig 7A and B). During mitotic process, RASSF7 was mainly present at the spindle pole regions where centrosomes localize (Fig 7C). We further overexpressed GFP-tagged Rassf7a into zebrafish embryos and found similar colocalization between Rassf7a and centrosome

proteins, γ -tubulin and Centrin (Appendix Fig S6, Movie EV9). Next, we performed knockdown analysis through siRNA approach. The knockdown efficiency was first evaluated by quantitative real-time PCR (Fig 7D). Similar to the NPCs in *rassf7a* mutants, the percentages of proliferating cells were significantly decreased in RASSF7 knockdown cells, as indicated by Ki67 or phospho-Histone H3 (pH3) antibody staining (Fig 7E–H). Further time-lapse imaging showed that the average cell division time was substantially delayed in the knockdown cells (Fig 7I and J, Movies EV10 and EV11). What's more, the percentages of dividing cells was also decreased

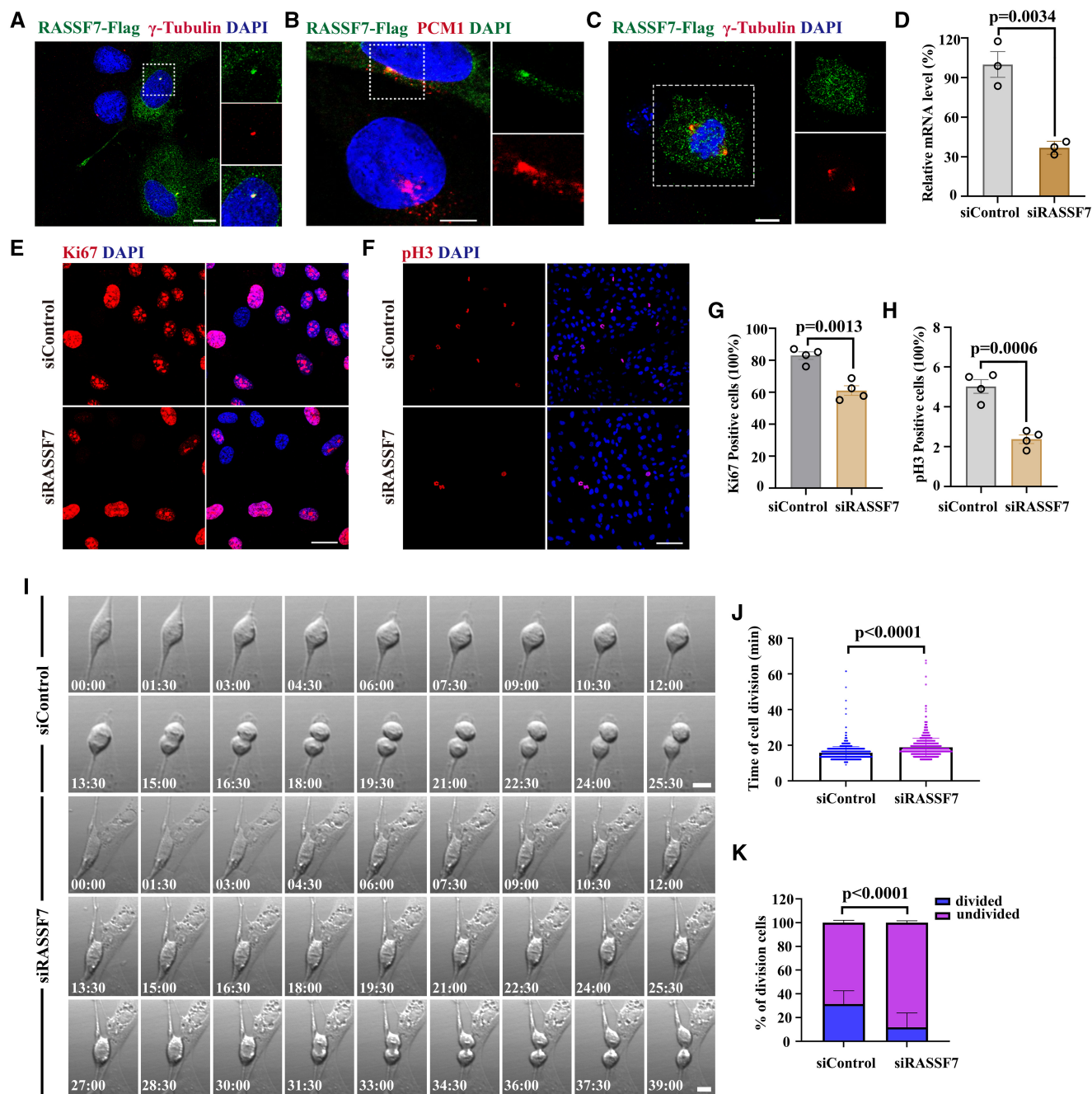


Figure 7. Knocking down of RASSF7 resulted in cell proliferation defects.

- A, B Subcellular localization of RASSF7 in hTERT-RPE-1 cells. The distribution of RASSF7 was visualized with anti-Flag antibody (green). The centrosome was stained by anti- γ -tubulin (red, A) and anti-PCMI (pericentriolar material 1) antibody (red, B), nuclei were labeled with DAPI (blue). $N = 3-6$ biological replicates per group.
- C During mitosis, localization of RASSF7 was enriched in the spindle poles (green), together with γ -tubulin (red). $N = 6$ biological replicates.
- D qRT-PCR results showing the relative expression level of RASSF7 in control or siRNA-treated cells $N = 3$ biological replicates per group. Each data point represents a biological replicate.
- E, F Representative staining results for Ki67 (red, E) and pH3 (red, F) positive cells in siRNA treated hTERT-RPE-1 cells.
- G, H Quantitative results of the percentages of Ki67 (G) and pH3 (H) positive cells in control or RASSF7 siRNA-treated cells. $N = 4$ biological replicates per group. Each data point in (G, H) represents a biological replicate.
- I Sequences of time-lapse photographs to illustrate mitotic divisions in control or RASSF7 siRNA-treated hTERT-RPE-1 cells.
- J Bar graph showing the time of cell division in control or RASSF7 siRNA treated cells. $N = 6$ biological replicates per group. Each data point represents a cell.
- K Bar graph showing percentages of divided cells in control or RASSF7 siRNA treated groups. $N = 6$ biological replicates per group.

Data information: P values for unpaired Student's t -test (D, G, H), Mann-Whitney test (J) and Fisher's Exact test (K) are indicated. Data are shown as mean \pm S.E.M. Scale bars: 20 μ m in (A, E), 8 μ m in (B), 7.5 μ m in (C), 100 μ m in (F), 10 μ m in (I).

when RASSF7 was depleted (Fig 7K). Thus, both *in vitro* and *in vivo* data suggested that RASSF7 played a critical role during cell proliferation.

Transcriptome analysis showed gene expression changes in *rassf7a* mutants after SCI

Next, we performed RNA transcriptome analysis on the injury sites of wild-type and *rassf7a* mutants at 3 days after injury. In wild-type larvae, we found about 1,288 differentially expressed genes (DEGs) at this time point of the regeneration process. By contrast, a total of 7,709 DEGs were found between the control and injured mutant groups, clearly suggesting that the whole gene regulatory network was significantly changed in the mutants (Appendix Fig S7A–C). Interestingly, we found many genes involved in cell cycle regulation were upregulated in wild-type larvae, but remained unchanged in the mutants, and some even showed decreased expression (Appendix Fig S7D). Similarly, we found the expression of genes involved in axon elongation or spindle polarity, such as *vangl2*, *pard3*, remain unchanged in the mutants, while the expression of these genes got increased after SCI in control siblings (Appendix Fig S7E and F). Thus, the RNA transcriptome analysis results further demonstrated expression changes of genes involved in cell proliferation and polarity regulation in the absence of Rassf7a after spinal cord injury.

Discussion

Spinal cord injury is a devastating trauma suffered by many people in the world. Unfortunately, neuron regeneration within the

injured spinal cord is still unfeasible in mammals and the underlying mechanisms remain poorly understood. By contrast, zebrafish exhibit high regeneration capacity after SCI, providing a powerful model to decode the mechanisms of spinal cord regeneration. Here, we showed that Rassf7a, a member of the Ras-association domain protein family, regulated spinal cord neurogenesis after SCI. Expression of *rassf7a* was restricted in the central nervous systems, with higher enrichment in the neural progenitor cells (Figs 1 and 4). Subcellular localization analysis suggested that Rassf7a was a centrosomal protein localized to the spindle pole during cell division. In agreement with this, Rassf7a deficiency resulted in spindle orientation defects during asymmetric division of NPCs. In zebrafish, as well as in mammals, the asymmetric division of NPCs gives rise to one neuronal cell and another NPC, which is the major pathway for newborn neuron development during neurogenesis. In the absence of Rassf7a, the asymmetric division characterized by the presence of cleavage planes perpendicular to the apical-basal axis of the radial-glia cells was significantly prohibited, thus less neurons could be generated. By contrast, NPCs were prone to undergo symmetric division in the mutants. Thus, the balance between symmetric and asymmetric division was disrupted in the mutants (Fig 8). In addition to that, the proliferation of NPCs was also prevented in the mutants as demonstrated from both live imaging and PCNA labeling assay. In such case, fewer neurons were generated in the mutants, leading to final regeneration defects.

How does Rassf7a influence spindle orientation? Spindle orientation is usually regulated by the astral microtubules through interaction with cell cortex. Interestingly, human RASSF7 protein was shown earlier to regulate cellular microtubule dynamics (Recino

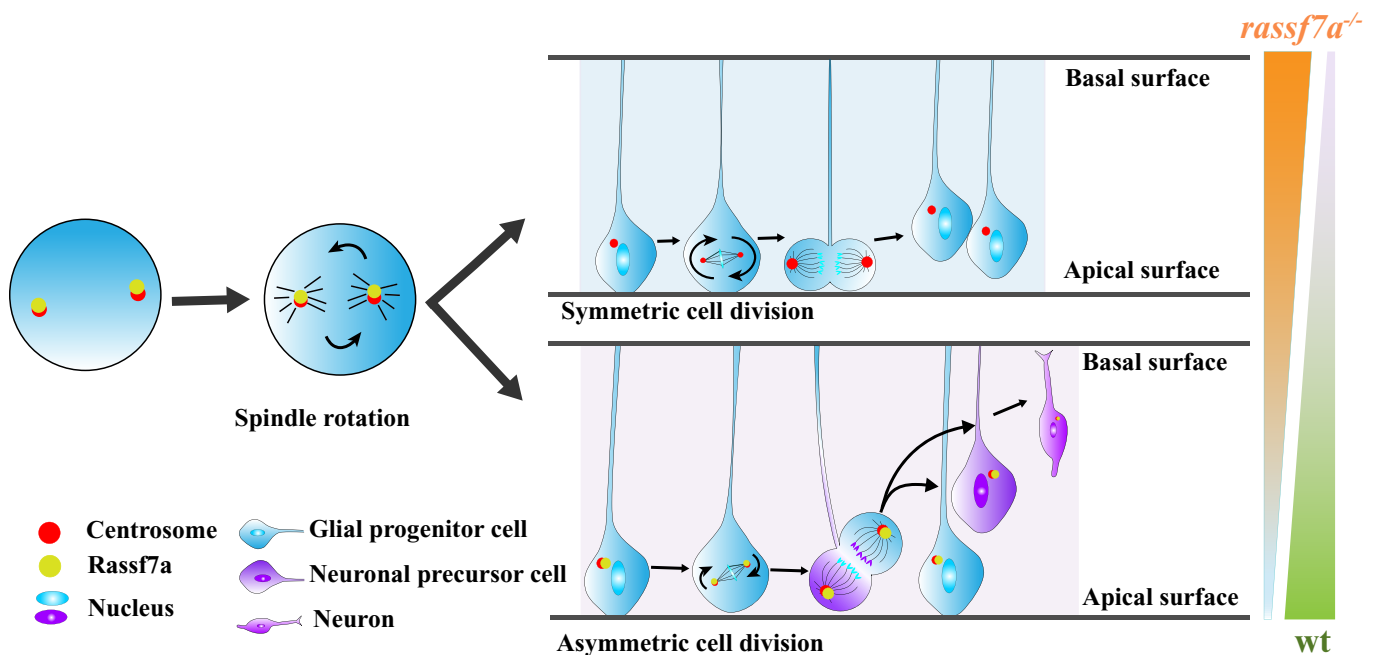


Figure 8. Model illustrating the role of Rassf7a during cell division of NPCs.

Rassf7a locates to the spindle pole and orchestrates spindle rotation during cell division of neural progenitor cells. Rassf7a deficiency results in spindle orientation defects characterized by increased rotation angles and decreased perpendicular (asymmetric) cell divisions (See Discussion).

et al, 2010; Takahashi et al, 2011; Wang et al, 2016). *Rassf7a* may regulate spindle orientation through mediating the pulling forces generated on the astral microtubules. The detailed regulatory mechanisms are still unknown. *Rassf7* has been shown earlier to regulate FGF/MEK/ERK signaling through binding to RAS proteins (Wang et al, 2016; Zhang et al, 2018a). Remarkably, the RAS-regulated ERK signaling is also vital for the spindle orientation during lung tube development, suggesting a similar role of FGF during spindle polarity establishment (Tang et al, 2011). It is conceivable that *Rassf7a* may function downstream of FGF signals to activate ERK signaling, which further influences centrosomal components of the mitotic spindle to organize spindle orientation.

Although *Rassf7a* was strongly expressed in the central nervous systems, CNS development is grossly normal in *rassf7a* mutant larvae (Appendix Fig S3A–E). Even in the absence of both *Rassf7a* and *Rassf7b* proteins, zebrafish mutants could still develop normally in larval stage. It is possible that other RASSF proteins compensate for the loss of *Rassf7* proteins, especially considering the highly conserved protein structures in this family (Richter et al, 2009; Underhill-Day et al, 2011). After acute spinal cord injury, neural progenitor cells undergo rapid cell proliferation, which may require a high level of *Rassf7* proteins to promote neurogenesis as suggested in Fig 4R. The gene regulation systems may fail to fully compensate for the loss of *Rassf7a* proteins which, eventually, leads to proliferation defects of neural progenitor cells, resulting in delayed axonal regeneration after SCI.

In summary, our data demonstrated the role of *Rassf7a* during the proliferation of neural progenitor cells after SCI. During spinal cord regeneration, neural progenitor cells represent one of the major resources for the generation of newborn neurons. Recently, transplantation of neural progenitor cells, or other stem cells, has shown promising therapeutic effects both in SCI animal models and human patients (Antonic et al, 2013; Chen et al, 2017). Our data provided a novel function of *Rassf7a* during the proliferation of neural progenitor cells in an animal model with high spinal cord regeneration capacity. Further in-depth studies on neuron differentiation mechanisms may help us find better ways to improve axonal regeneration and motor function in SCI patients.

Materials and Methods

Ethics statement

All zebrafish study was conducted according standard animal guidelines and approved by the Animal Care Committee of Ocean University of China (Animal protocol number: OUC2012316).

Animals

All zebrafish strains were maintained at 28°C on a 14-h (h) light/10-h dark cycle. Embryos were raised at 28.5°C in E3 medium (5 mM NaCl, 0.17 mM KCl, 0.39 mM CaCl₂, 0.67 mM MgSO₄) following standard protocols. CRISPR/Cas9 technology was used to generate zebrafish *rassf7a* mutants with the following target site for single guide (sg) RNA (5'-AGTCCAAGCAGGGTTACCT-3'). The *rassf7b* mutant strain was constructed using the TALEN system with the following binding sequences: 5'-TATGTTCTCATCCAGAAAC-3' and 5'-

GGCAGCTTATGGCCAATGA-3'. The sgRNA synthesis and TALEN plasmids constructions were similar to previously described (Zhang et al, 2018b). The primer sequences used for mutant detection were listed in Appendix Table S1. The Tg(*huc:GFP*) and Tg(*gfap:GFP*) transgenes were gifts from Dr. Jiulin Du (Institute of Neuroscience, Shanghai), the Tg(*sox2:sox2-2a-sfGFP*) was a gift from Dr. Lilianna Solnica-Krezel. The Tg(*foxj1a:HA-tdTomato*) was generated using Multisite Gateway recombination with the following constructs: pDEST vector, p5e-*foxj1a*, pDONR221-*HA-tdTomato* and p3e-polyA. Multisite gateway cloning was performed according to the standard protocol from Invitrogen (Life Technologies).

In situ hybridization

Full length or partial cDNA fragments were PCR amplified from a 24 hpf wild-type zebrafish cDNA library and cloned into pGEM-T vector. The primer sequences used for PCR amplification were listed in Appendix Table S1. Probe preparation and whole mount *in situ* hybridization were carried out following standard protocols. For fluorescence *in situ* hybridization, zebrafish embryos were first incubated with digoxigenin- and fluorescein-labeled RNA probes, then followed by sequential detection using POD labeled anti-Digoxigenin and POD labeled anti-Fluorescein antibodies. Briefly, embryos were first incubated with probes for hybridization, then serially washed with 50% formamide/2 × SSCT, 2 × SSCT, 0.2 × SSCT, MABT (100 mM Maleic acid, 150 mM NaCl, 1% Tween-20) and PBST. After that, embryos were refixed in 4% PFA for 4 h at room temperature (RT), cryoprotected in 30% sucrose at 4°C overnight, then further processed for cryosectioning. After briefly washing with PBST and MABT, slides were blocked in blocking solution for 30 min at RT, then incubated with POD labeled anti-Digoxigenin antibody at 4°C overnight. Next day, the digoxigenin-labeled probe was first detected with TSA Plus Cy3 Solution (Perkin Elmer). After signal quenching steps, the slides were incubated again with POD labeled anti-Fluorescein antibody at 4°C overnight. Finally, the slides were washed and detected with TSA Plus Fluorescein solution (Perkin Elmer). The staining images were captured with Leica SP8 confocal microscope.

Spinal cord injury

Three dpf zebrafish larvae were first anesthetized with 0.01% Tricaine in E3 water, then placed on another Petri dish to remove excess medium. The spinal cord was transected with a beveled microinjection pipette at the dorsal site above the end of the yolk extension, and the notochord and major blood vessels should be intact to ensure a > 95% survival rate at 5 dpi for both mutant and control larvae. After injury, the larvae were placed in a 96-well plate with fresh E3-water to recover for 2 h. Then, the dead larvae were removed and survived larvae were changed with fresh E3 water, and cultured for further analysis (Fig EV1A and B).

Locomotion behavior assessment

Individual zebrafish larva was transferred into 24-well plate with fresh E3 medium at 6 days after injury. Then, the plate was placed inside the Daniovision (Noldus) observation chamber for further behavior analysis. Video-tracking of swimming activity, tapping

stimulation experiments and further statistical analysis were performed using the EthoVision™ XT10 software. Behavioral data were shown as total swim distance (cm), average velocity (cm/s) and cumulative duration time (s) at a duration for 500 s or 300 s.

BrdU labeling and immunohistochemistry

For BrdU labeling assay, 10–15 embryos were first transferred into 48-well plate shortly after injury, or at 2 and 4 days after injury, then incubated with 10 mM BrdU (Invitrogen) in E3 culture medium for 1 h at 28.5°C. After that, the culture medium was replaced with fresh E3 medium for 24 h, then the treated larvae were fixed with 4% PFA overnight at 4°C. After briefly wash with PBST, the fixed larvae were cryoprotected in 30% sucrose overnight. Approximately 800 µm fragments located proximal to the damaged site from both sides of the lesion were collected and embedded in OCT medium. Coronal sections were collected from dorsal to ventral at 14 µm thickness on a Leica CM1850 cryostat. Sections were further incubated in 2 N HCl for 90 min at room temperature, then proceeded for immunostaining. For PCNA antibodies immunofluorescence staining, embryos were fixed in 4% PFA at 4°C overnight, then embryos were further proceeded for cryosectioning. Antigen retrieval was performed on sections by incubating with 10 mM sodium citrate for 30 min at 65°C, followed by regular immunostaining protocol. Immunohistochemistry on whole-mount larvae and cryosections were performed as previously described (Leventea et al, 2016). The following antibodies were used: rabbit anti-acetylated α Tubulin (1:500, Cell Signaling Technology), rabbit anti-Sox2 (1:500, Abcam), mouse anti-BrdU (1:500, Invitrogen), mouse anti-PCNA (1:500, Sigma), rabbit anti- γ -Tubulin (1:2,000, Sigma-Aldrich), mouse anti-Flag (1:200, Sigma-Aldrich), rabbit anti-PCMI (1:1,000, Cell Signaling Technology), rabbit anti-Ki67 (1:300, Abcam), rabbit anti-pH3 (1:500, Bethyl Laboratories).

Overexpression and knockdown experiments

For rescue experiments, full-length *rassf7a* gene was first cloned into pDONR221 Gateway entry vector, then final construct was made by Multisite Gateway technology with the following vectors: p5e-*hsp70l*, pDONR221-*rassf7a*, p2rp3-*HA-tdTomato* and pDestTol2. For control experiments, the pDONR221-*rassf7a*, p2rp3-*HA-tdTomato* was replaced by pDONR221-*HA-tdTomato*, p3e-polyA respectively. Both *rassf7a* and control plasmids were microinjected into single-cell stage embryos at a concentration of 40 ng/µl, together with 50 ng/µl transposase mRNA. The injected embryos were first heat induced at 24 hpf for 4 h at 37°C, then fluorescent embryos were collected and further transferred into a new Petri dish containing fresh E3 medium. These embryos were further maintained at 28.5°C. At 3 dpf, embryos were heat induced at 37°C for 4 h, then followed by spinal cord injury. After that, embryos were maintained at 28.5°C and heat induced every day for 2 h periodically until further analysis.

To knockdown the expression of *rassf7a* in wild-type larvae, 1 µl of *rassf7a* vivo morpholino (5'-AGCTCCATCAGAGGCCACCAAGCACA-3') was injected at both sides of the lesion site at a concentration of 0.25 mM immediately after SCL. A standard control vivo morpholino (5'-CCTCTTACCTCAGTTACAATTTATA-3') was injected similarly. The injected larvae were collected at different

time points after injury for further analysis. To verify the efficiency of *rassf7a* morpholino, we first cloned the exon of *rassf7a* containing the translation start site and morpholino binding site, and then fused in frame to the N-terminus of GFP driven by a CMV promoter. The report construct was injected together with *rassf7a* or control morpholinos to test the expression of GFP. The primer sequences used for generating the constructs were listed in Appendix Table S1.

Fluorescence-activated cell sorting (FACS)

To isolated single cells expressing Huc or Sox2, about one hundred 3 dpf zebrafish larvae carrying Tg(*huc:GFP*) or Tg(*sox2:sox2-2a-sfGFP*) transgene were first anesthetized and decapitated with tweezers. The trunk containing the whole spinal cord was transferred into 1.5 ml microcentrifuge tubes (50 larvae per tube), then washed with Dulbecco's Phosphate Buffered Saline (D-PBS) without calcium and magnesium (Sangon Biotech, # E607009). After briefly dissociated with 1 ml pipet tips, 60 µl 0.25% trypsin was added to the tube and incubated at 37°C for 20 min. After that, the digestion reaction was stopped by adding 600 µl DMEM containing 30% FBS for 5 min, then centrifuged at 700 g for 5 min. After briefly wash with D-PBS, the cell suspension was filtered with 40 µm nylon mesh (Sangon Biotech, # F613461). The GFP-positive cells were collected using WOLF G2 (NanoCollect) or BD FACSaria II (BD Biosciences). Total RNA from 1×10^6 sorting cells was extracted with the RNAqueous™-Micro Total RNA Isolation Kit (ThermoFisher, # AM1931).

Quantitative RT-PCR

Reverse transcription of RNA was performed with HiScript III RT SuperMix for qPCR kit (Vazyme, # R323-01). qRT-PCR was set up using the Eva-Green Master Mix (ABM) and performed on the StepOne real-time PCR system (Thermo Scientific). The amplification condition parameters were 95°C for 15 s, followed by 40 cycles of 95°C for 5 s, 60°C for 15 s, and 72°C for 35 s. Each samples had triplicate reactions. Relative gene expression levels were quantified using the comparative C_T method ($2^{-\Delta\Delta C_T}$ method) on the basis of C_T values for target genes and zebrafish β -actin. Primer were designed to span an exon–exon junction using Oligo 7 software. Primer sequences are listed in Appendix Table S1.

RNA-seq transcriptome analysis

The trunk regions covering the injury sites were collected from 50 larvae at 3 dpi and immediately transferred into Trizol solution (Takara). Total RNAs were isolated from these samples in triplicate. Bulk RNA sequencing was performed by Novogene using Illumina HiSeq X Ten (Novogene Bioinformatics Technology Co., Ltd., Tianjin, China). Data processing was similar to previously described (Xie et al, 2020).

Cell culture and knockdown analysis

The hTERT-RPE-1 cells were grown in DMEM/F12 (Gibco) media supplemented with 10% fetal bovine serum (FBS; Gibco, Grand Island, NY, USA) and 100 IU/ml of penicillin/streptomycin (Gibco), and maintained at 37°C in a humidified incubator supplied with 5%

CO₂. The expression vector RASSF7-Flag plasmid was transfected with plasmids psPAX2 and pMD2.G (Addgene) into HEK293T cells following previously described protocols (Luo *et al*, 2021). The supernatant containing virus was filtered through a 0.45- μ m membrane and then was added to RPE-1 cells with 6 μ g/ml of polybrene (sc-134220; Santa Cruz). Forty-eight hours later, fresh medium containing 8 μ g/ml puromycin was added to replace the virus-containing medium. Puromycin selection lasted for 2 weeks. The stable line was then used for subcellular localization analysis. For knockdown assay, the transfections of siRNAs were performed using Lipofectamine RNAiMAX (13778; Invitrogen). The final concentrations of siRNAs were 30 nM. Control siRNA and RASSF7 siRNA were obtained from Dharmacon, the siRNA sequence of RASSF7 was: 5'-UAAUUCGUGCCAGCCUCCUGUAAA-3', a general sequence of 5'-UUCUCCGACGUGUCACGU-3' was used as a negative control.

For live-cell time-lapse study, cells treated with RASSF7 siRNA (siRASSF7) or control siRNA (siControl) for 48 h, and then maintained at 37°C in fresh medium (Invitrogen) and monitored with a spinning disk confocal microscopy (Leica) equipped with a temperature-controlled apparatus. DIC (Differential Interference Contrast) still time-lapse images were acquired with 20 \times /0.55 objective in multi-position mode, at 1 μ m spacing and 1,024 \times 1,024-pixel resolution every 90 s for 12 h using Andor Dragonfly 200 high speed confocal platform system and Andor IXON-L-888 EMCCD camera controlled by Andor Fusion software. The movies were generated using the Image J software (NIH Image, Bethesda, MD, USA).

Time-lapse imaging and spindle orientation analysis

The Tg(*sox2:sox2-2a-sfGFP*) knockin transgenic larvae were microinjected with control or *rassf7a* vivo morpholino immediately after spinal cord injury. At 1 dpi, the larvae were anesthetized with 0.16 mg/ml Tricaine (Sigma), mounted in 1% low melting-point agarose (Sigma) in glass-bottom dishes (FD35-100, WPI), then covered with E3 water containing 0.04 mg/ml Tricaine. Time-lapse images were collected with IXON-L-888 EMCCD camera equipped on Dragonfly 200 Spinning Disk Confocal Microscope using a 40 \times /1.10 water objective. Z-stack images were collected every 90 s for a duration of 12 h. Images were further analyzed with Fusion or ImageJ software.

To quantify spindle rotation, the angles were calculated between the longer axis of metaphase and anaphase stages (Fig 5B). For spindle orientation analysis, we drew a line across the spindle poles at mitosis telophase stage, and considered the angle between this line and antero-posterior axis as a criterion for spindle orientation (Fig 6B). Spindle orientation in control and *rassf7a* mutant or morphant cells were quantified using ImageJ software.

To trace the symmetric and asymmetric division of neural progenitor cells, zebrafish embryos carrying Tg(*huc:Gal4;uas-mcherry*) transgene were microinjected with *H2B-GFP* mRNA at one cell stage. At 24 hpf, the embryos were anesthetized with 0.16 mg/ml Tricaine, mounted in 1% low melting-point agarose (Sigma) in glass-bottom dishes (FD35-100, WPI), then covered with E3 water containing 0.04 mg/ml Tricaine. Time-lapse images were collected with IXON-L-888 EMCCD camera equipped on Dragonfly 200 Spinning Disk Confocal Microscope using a 40 \times /1.10 water objective. Z-stack images were collected every 90 s for a duration of 8–12 h. Images were further analyzed with Fusion or ImageJ software.

Quantifications and statistical analysis

To measure GFP expression level at the lesion sites, we first took both bright field and fluorescence images using Leica M165FC stereomicroscope with the same magnification. Then, a 837 μ m \times 417 μ m area covering the entire lesion site of each zebrafish larva was selected to measure the green fluorescence area (Fig 2A). The areas of GFP expression and entire neural tube (red dashed box in Fig 2A) were measured from each fluorescence and bright field image using ImageJ software, and the ratios were used to evaluate the regeneration efficiency of each zebrafish larva.

For cell proliferation assay, we selected a grid (200 μ m²) next to the injury sites (within 300 μ m) on the coronal sections of the spinal cord. Within each grid, the number of cells that were labeled with both BrdU (or PCNA) and GFP was counted using Adobe Photoshop CS6. The ratio of these double labeled cells to single GFP-positive cells within the selected area was calculated for each larva to evaluate cell proliferating levels.

The quantification of axonal and glial fascicle was performed following previous studies (Wehner *et al*, 2017). Briefly, fascicles were identified as fluorescent protrusions that projected into the injury site for at least 20 μ m or completely through the injury site. The fascicles containing both glial and neuronal fluorescence expression were classified as “mixed,” otherwise were classified as purely “axonal” or “glial”.

All experiments were performed at least three times. The quantitative data were tested for normality and analyzed with parametric and non-parametric tests as appropriate. Analysis of the data were not randomized or blinded. All the statistical methods used were indicated in each figure legend and summarized in Appendix Table S2. Differences were considered statistically significant at *P* values below 0.05. Variance for all groups data is presented as \pm standard error of the mean (S.E.M.). Graphs were generated using GraphPad Prism 8.0.2 and SPSS Statistics 23.0.

Data availability

Bulk RNA-seq data has been deposited to the Sequence Read Archive (SRA) database under accession numbers PRJNA876641 (<https://www.ncbi.nlm.nih.gov/bioproject/PRJNA876641>). The single-cell RNA sequencing datasets used in Fig EV4 were from two published single-cell transcriptomes (accession number: E-MTAB-10390: <https://www.ebi.ac.uk/biostudies/arrayexpress/studies/E-MTAB-10390> and GSE173350: <https://www.ncbi.nlm.nih.gov/geo/query/acc.cgi?acc=GSE173350>).

Expanded View for this article is available [online](#).

Acknowledgements

The authors thank Dr. Lilianna Solnica-Krezel for providing the Tg(*sox2:sox2-2a-sfGFP*) knockin transgenic line, Dr. Jiulin Du for providing the Tg(*huc:GFP*) and Tg(*gfap:GFP*) zebrafish lines, and Dr. Brian Ciruna and Dr. Seok-Yong for providing the *p5E-foxj1a* plasmid. We also thanks Dr. Hongyan Li for the excellent support of the *rassf7b* TALEN experiments, and Dr. Linjia Jiang, Dr. Dong Liu, Dr. Jifeng Fei and Dr. Wei Wang for their kind help on the preparation of this manuscript. This work was supported by the National Natural Science Foundation of China (Nos. 31991194, 32125015) to CZ and the National Key Research and

Development Program of China (2021YFC2700800), the National Natural Science Foundation of China (91954123 and 31972887), Shanghai Science and Technology Commission (20JC1410100), and Innovative research team of high-level local universities in Shanghai (SHSMU-ZDCX20211800) to MC.

Author contributions

Panpan Zhu: Data curation; software; formal analysis; validation; investigation; visualization; methodology; writing – original draft.
Pengfei Zheng: Data curation; software; formal analysis; validation; visualization; methodology. **Xinlong Kong:** Validation; visualization; methodology. **Shuo Wang:** Software; investigation; visualization; methodology. **Muqing Cao:** Funding acquisition; methodology; writing – original draft; writing – review and editing. **Chengtian Zhao:** Conceptualization; supervision; funding acquisition; writing – original draft; project administration; writing – review and editing.

Disclosure and competing interests statement

The authors declare that they have no conflict of interest.

References

- Ahuja CS, Wilson JR, Nori S, Kotter MRN, Druschel C, Curt A, Fehlings MG (2017) Traumatic spinal cord injury. *Nat Rev Dis Primers* 3: 17018
- Alexandre P, Reugels AM, Barker D, Blanc E, Clarke JD (2010) Neurons derive from the more apical daughter in asymmetric divisions in the zebrafish neural tube. *Nat Neurosci* 13: 673–679
- Antonic A, Sena ES, Lees JS, Wills TE, Skeers P, Batchelor PE, Macleod MR, Howells DW (2013) Stem cell transplantation in traumatic spinal cord injury: a systematic review and meta-analysis of animal studies. *PLoS Biol* 11: e1001738
- Becker CG, Becker T (2015) Neuronal regeneration from ependymo-radial glial cells: cook, little pot, cook! *Dev Cell* 32: 516–527
- Becker CG, Lieberoth BC, Morellini F, Feldner J, Becker T, Schachner M (2004) L1.1 is involved in spinal cord regeneration in adult zebrafish. *J Neurosci* 24: 7837–7842
- Becker CG, Becker T, Hugnot JP (2018) The spinal ependymal zone as a source of endogenous repair cells across vertebrates. *Prog Neurobiol* 170: 67–80
- Bhatt DH, Otto SJ, Depoister B, Fetcho JR (2004) Cyclic AMP-induced repair of zebrafish spinal circuits. *Science* 305: 254–258
- Bradbury EJ, Burnside ER (2019) Moving beyond the glial scar for spinal cord repair. *Nat Commun* 10: 3879
- Briona LK, Dorsky RI (2014) Radial glial progenitors repair the zebrafish spinal cord following transection. *Exp Neurol* 256: 81–92
- Briona LK, Poulain FE, Mosimann C, Dorsky RI (2015) Wnt/ss-catenin signaling is required for radial glial neurogenesis following spinal cord injury. *Dev Biol* 403: 15–21
- Bultje RS, Castaneda-Castellanos DR, Jan LY, Jan YN, Kriegstein AR, Shi SH (2009) Mammalian Par3 regulates progenitor cell asymmetric division via notch signaling in the developing neocortex. *Neuron* 63: 189–202
- Cavone L, McCann T, Drake LK, Aguzzi EA, Oprisoreanu AM, Pedersen E, Sandi S, Selvarajah J, Tsarouchas TM, Wehner D et al (2021) A unique macrophage subpopulation signals directly to progenitor cells to promote regenerative neurogenesis in the zebrafish spinal cord. *Dev Cell* 56: 1617–1630
- Chen B, Xiao Z, Zhao Y, Dai J (2017) Functional biomaterial-based regenerative microenvironment for spinal cord injury repair. *Natl Sci Rev* 4: 530–532
- Dias TB, Yang YJ, Ogai K, Becker T, Becker CG (2012) Notch signaling controls generation of motor neurons in the lesioned spinal cord of adult zebrafish. *J Neurosci* 32: 3245–3252
- Dong Z, Yang N, Yeo SY, Chitnis A, Guo S (2012) Intralineage directional notch signaling regulates self-renewal and differentiation of asymmetrically dividing radial glia. *Neuron* 74: 65–78
- Essner JJ, Amack JD, Nyholm MK, Harris EB, Yost HJ (2005) Kupffer's vesicle is a ciliated organ of asymmetry in the zebrafish embryo that initiates left-right development of the brain, heart and gut. *Development* 132: 1247–1260
- Fededa JP, Esk C, Mierzwa B, Stanyte R, Yuan S, Zheng H, Ebnet K, Yan W, Knoblich JA, Gerlich DW (2016) MicroRNA-34/449 controls mitotic spindle orientation during mammalian cortex development. *EMBO J* 35: 2386–2398
- Fei JF, Schuez M, Tazaki A, Taniguchi Y, Roensch K, Tanaka EM (2014) CRISPR-mediated genomic deletion of Sox2 in the axolotl shows a requirement in spinal cord neural stem cell amplification during tail regeneration. *Stem Cell Reports* 3: 444–459
- Ghosh S, Hui SP (2018) Axonal regeneration in zebrafish spinal cord. *Regeneration (Oxf)* 5: 43–60
- Goldshmit Y, Sztal TE, Jusuf PR, Hall TE, Nguyen-Chi M, Currie PD (2012) Fgf-dependent glial cell bridges facilitate spinal cord regeneration in zebrafish. *J Neurosci* 32: 7477–7492
- Goldshmit Y, Frisca F, Pinto AR, Pebay A, Tang JK, Siegel AL, Kaslin J, Currie PD (2014) Fgf2 improves functional recovery-decreasing gliosis and increasing radial glia and neural progenitor cells after spinal cord injury. *Brain Behav* 4: 187–200
- Goldshmit Y, Tang J, Siegel AL, Nguyen PD, Kaslin J, Currie PD, Jusuf PR (2018) Different Fgfs have distinct roles in regulating neurogenesis after spinal cord injury in zebrafish. *Neural Dev* 13: 24
- Graham V, Khudyakov J, Ellis P, Pevny L (2003) SOX2 functions to maintain neural progenitor identity. *Neuron* 39: 749–765
- Gulsten T, Hadjicosti I, Li Y, Zhang X, Whitley PR, Chalmers AD (2016) Truncated RASSF7 promotes centrosomal defects and cell death. *Dev Biol* 409: 502–517
- Han X, Xie H, Wang Y, Zhao C (2018) Radial spoke proteins regulate otolith formation during early zebrafish development. *FASEB J* 32: 3984–3992
- Haydar TF, Ang E Jr, Rakic P (2003) Mitotic spindle rotation and mode of cell division in the developing telencephalon. *Proc Natl Acad Sci U S A* 100: 2890–2895
- Hui SP, Dutta A, Ghosh S (2010) Cellular response after crush injury in adult zebrafish spinal cord. *Dev Dyn* 239: 2962–2979
- Hui SP, Nag TC, Ghosh S (2015) Characterization of proliferating neural progenitors after spinal cord injury in adult zebrafish. *PLoS One* 10: e0143595
- Kaltschmidt JA, Davidson CM, Brown NH, Brand AH (2000) Rotation and asymmetry of the mitotic spindle direct asymmetric cell division in the developing central nervous system. *Nat Cell Biol* 2: 7–12
- Kitagawa D, Kajihio H, Negishi T, Ura S, Watanabe T, Wada T, Ichijo H, Katada T, Nishina H (2006) Release of RASSF1C from the nucleus by Daxx degradation links DNA damage and SAPK/JNK activation. *EMBO J* 25: 3286–3297
- Klatt Shaw D, Saraswathy VM, Zhou L, McAdow AR, Burris B, Butka E, Morris SA, Dietmann S, Mokalled MH (2021) Localized EMT reprograms glial progenitors to promote spinal cord repair. *Dev Cell* 56: 613–626
- Ko CC, Tu TH, Wu JC, Huang WC, Tsai YA, Huang SF, Huang HC, Cheng H (2018) Functional improvement in chronic human spinal cord injury: four years after acidic fibroblast growth factor. *Sci Rep* 8: 12691
- Konno D, Shioi G, Shitamukai A, Mori A, Kiyonari H, Miyata T, Matsuzaki F (2008) Neuroepithelial progenitors undergo LGN-dependent planar

- divisions to maintain self-renewability during mammalian neurogenesis. *Nat Cell Biol* 10: 93–101
- Leventea E, Hazime K, Zhao C, Malicki J (2016) Analysis of cilia structure and function in zebrafish. *Methods Cell Biol* 133: 179–227
- Luo M, Lin Z, Zhu T, Jin M, Meng D, He R, Cao Z, Shen Y, Lu C, Cai R et al (2021) Disrupted intraflagellar transport due to IFT74 variants causes Joubert syndrome. *Genet Med* 23: 1041–1049
- Mokalled MH, Patra C, Dickson AL, Endo T, Stainier DY, Poss KD (2016) Injury-induced *ctgfa* directs glial bridging and spinal cord regeneration in zebrafish. *Science* 354: 630–634
- Ogai K, Nakatani K, Hisano S, Sugitani K, Koriyama Y, Kato S (2014) Function of Sox2 in ependymal cells of lesioned spinal cords in adult zebrafish. *Neurosci Res* 88: 84–87
- Ohnmacht J, Yang Y, Maurer GW, Barreiro-Iglesias A, Tsarouchas TM, Wehner D, Sieger D, Becker CG, Becker T (2016) Spinal motor neurons are regenerated after mechanical lesion and genetic ablation in larval zebrafish. *Development* 143: 1464–1474
- O'Shea TM, Burda JE, Sofroniew MV (2017) Cell biology of spinal cord injury and repair. *J Clin Invest* 127: 3259–3270
- Postiglione MP, Juschke C, Xie Y, Haas GA, Charalambous C, Knoblich JA (2011) Mouse *inscuteable* induces apical-basal spindle orientation to facilitate intermediate progenitor generation in the developing neocortex. *Neuron* 72: 269–284
- Recino A, Sherwood V, Flaxman A, Cooper WN, Latif F, Ward A, Chalmers AD (2010) Human RASSF7 regulates the microtubule cytoskeleton and is required for spindle formation, Aurora B activation and chromosomal congression during mitosis. *Biochem J* 430: 207–213
- Reimer MM, Sorensen I, Kuscha V, Frank RE, Liu C, Becker CG, Becker T (2008) Motor neuron regeneration in adult zebrafish. *J Neurosci* 28: 8510–8516
- Richter AM, Pfeifer GP, Dammann RH (2009) The RASSF proteins in cancer; from epigenetic silencing to functional characterization. *Biochim Biophys Acta* 1796: 114–128
- Schwab ME, Bartholdi D (1996) Degeneration and regeneration of axons in the lesioned spinal cord. *Physiol Rev* 76: 319–370
- Scott K, O'Rourke R, Winkler CC, Kearns CA, Appel B (2021) Temporal single-cell transcriptomes of zebrafish spinal cord pMN progenitors reveal distinct neuronal and glial progenitor populations. *Dev Biol* 479: 37–50
- Shao W, Yang J, He M, Yu XY, Lee CH, Yang Z, Joyner AL, Anderson KV, Zhang J, Tsou MB et al (2020) Centrosome anchoring regulates progenitor properties and cortical formation. *Nature* 580: 106–112
- Sherwood V, Manbodr R, Sheppard C, Chalmers AD (2008) RASSF7 is a member of a new family of RAS association domain-containing proteins and is required for completing mitosis. *Mol Biol Cell* 19: 1772–1782
- Shin J, Chen J, Solnica-Krezel L (2014) Efficient homologous recombination-mediated genome engineering in zebrafish using TALE nucleases. *Development* 141: 3807–3818
- Shohayeb B, Muzar Z, Cooper HM (2021) Conservation of neural progenitor identity and the emergence of neocortical neuronal diversity. *Semin Cell Dev Biol* 118: 4–13
- Silver J, Miller JH (2004) Regeneration beyond the glial scar. *Nat Rev Neurosci* 5: 146–156
- Song Z, Zhang X, Jia S, Yelick PC, Zhao C (2016) Zebrafish as a model for human ciliopathies. *J Genet Genomics* 43: 107–120
- Strand NS, Hoi KK, Phan TMT, Ray CA, Berndt JD, Moon RT (2016) Wnt/beta-catenin signaling promotes regeneration after adult zebrafish spinal cord injury. *Biochem Biophys Res Commun* 477: 952–956
- Suzuki M, Satoh A, Ide H, Tamura K (2005) Nerve-dependent and -independent events in blastema formation during xenopus froglet limb regeneration. *Dev Biol* 286: 361–375
- Takahashi S, Ebihara A, Kajiho H, Kontani K, Nishina H, Katada T (2011) RASSF7 negatively regulates pro-apoptotic JNK signaling by inhibiting the activity of phosphorylated-MKK7. *Cell Death Differ* 18: 645–655
- Tang N, Marshall WF, McMahon M, Metzger RJ, Martin GR (2011) Control of mitotic spindle angle by the RAS-regulated ERK1/2 pathway determines lung tube shape. *Science* 333: 342–345
- Tazaki A, Tanaka EM, Fei JF (2017) Salamander spinal cord regeneration: the ultimate positive control in vertebrate spinal cord regeneration. *Dev Biol* 432: 63–71
- Tsata V, Mollmert S, Schweitzer C, Kolb J, Mockel C, Bohm B, Rosso G, Lange C, Lesche M, Hammer J et al (2021) A switch in *pdgfrb(+)* cell-derived ECM composition prevents inhibitory scarring and promotes axon regeneration in the zebrafish spinal cord. *Dev Cell* 56: 509–524
- Underhill-Day N, Hill V, Latif F (2011) N-terminal RASSF family (RASSF7-RASSF10) a mini review. *Epigenetics* 6: 284–292
- Wang SK, Liang QL, Qiao HM, Li H, Shen TJ, Ji F, Jiao JW (2016) DISC1 regulates astrogenesis in the embryonic brain via modulation of RAS/MEK/ERK signaling through RASSF7. *Development* 143: 2732–2740
- Wehner D, Tsarouchas TM, Michael A, Haase C, Weidinger G, Reimer MM, Becker T, Becker CG (2017) Wnt signaling controls pro-regenerative collagen XII in functional spinal cord regeneration in zebrafish. *Nat Commun* 8: 126
- Xie H, Kang Y, Wang S, Zheng P, Chen Z, Roy S, Zhao C (2020) E2f5 is a versatile transcriptional activator required for spermatogenesis and multiciliated cell differentiation in zebrafish. *PLoS Genet* 16: e1008655
- Zhang M, Li Q, Zhang L, Wang Y, Wang L, Li Q, He T, Wan B, Wang X (2018a) RASSF7 promotes cell proliferation through activating MEK1/2-ERK1/2 signaling pathway in hepatocellular carcinoma. *Cell Mol Biol (Noisy-le-Grand)* 64: 73–79
- Zhang X, Jia S, Chen Z, Chong YL, Xie H, Feng D, Wu X, Song DZ, Roy S, Zhao C (2018b) Cilia-driven cerebrospinal fluid flow directs expression of urotensin neuropeptides to straighten the vertebrate body axis. *Nat Genet* 50: 1666–1673
- Zhao CT, Malicki J (2007) Genetic defects of pronephric cilia in zebrafish. *Mech Dev* 124: 605–616

Expanded View Figures

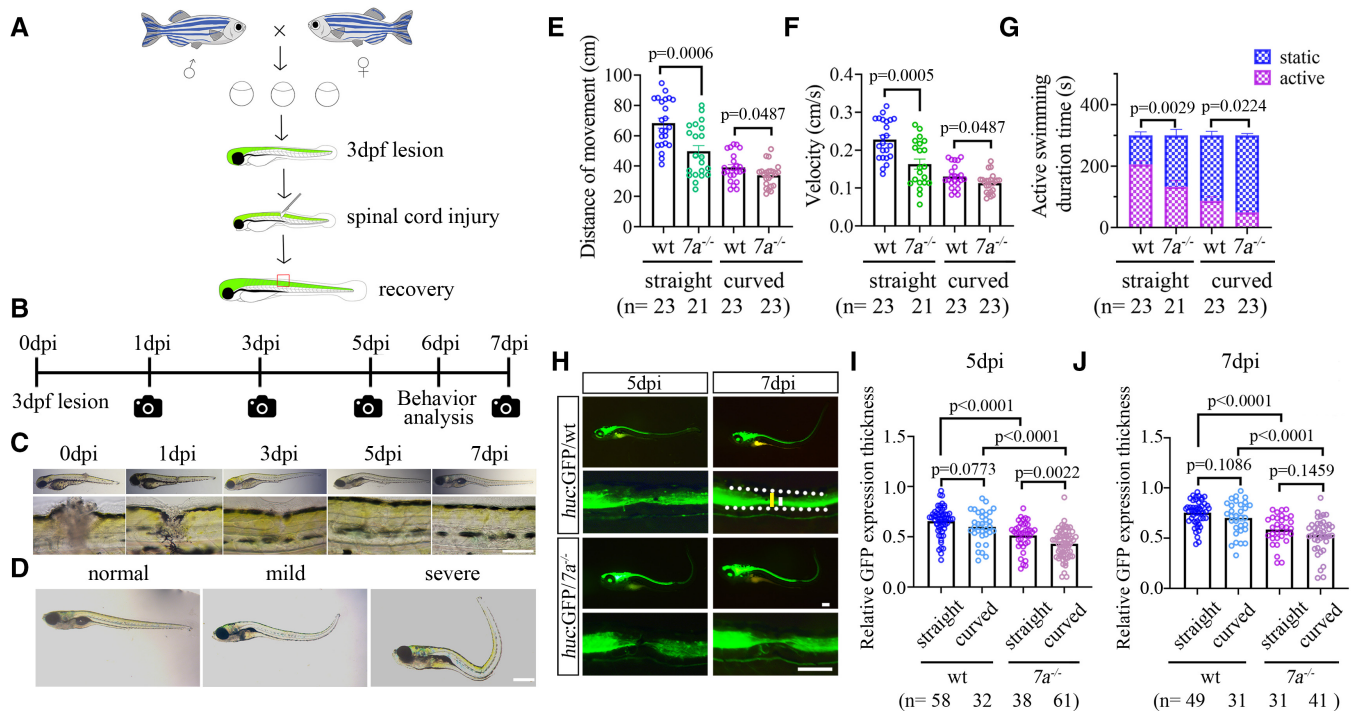


Figure EV1. Strategies of examining spinal cord regeneration after SCI.

A Diagram showing that transgenic zebrafish larva was injured at the trunk spinal cord at 3 dpf and recovered later during development.

B Timeline of imaging and behavior analysis of zebrafish larvae after SCI at 3 dpf.

C Representative images showing the recovery of a wild-type zebrafish larva injured at 3 dpf. Bottom images showing the enlarged views of the lesion sites.

D Representative images showing the external phenotypes of three categories of larvae at 6 dpi.

E Dot plots showing the swimming distance of each larva in different groups as indicated at a duration of 300 s.

F Dot plots showing the swimming velocity of wild-type and mutant larvae as indicated.

G Bar graph showing active swimming time in wild-type and mutant larvae in different groups as indicated at a duration of 300 s.

H Representative images showing GFP expression in wild-type or *rassf7a* mutants carrying Tg(*huc:GFP*) transgene at different time points after SCI. Bottom rows show the magnified views near the lesion sites. The white dashed border represents the entire spinal cord near the lesion sites. Long line in yellow indicates measurement of spinal cord thickness. Short line in white indicates the measurement of GFP fluorescence thickness.

I, J Dot plots showing relative thickness of GFP fluorescence at the lesion sites of wild-type or mutant larvae at 5 dpi (I) and 7 dpi (J) in different groups as indicated.

Data information: *P* values for unpaired Student's *t*-test (E-F, J), unpaired Mann–Whitney test (I) and Two-way ANOVA with Bonferroni's multiple comparisons test (G) are indicated. Data are shown as mean \pm S.E.M. Each data point represents an individual fish. Scale bars: 500 μ m in (C, D), 250 μ m in (H).

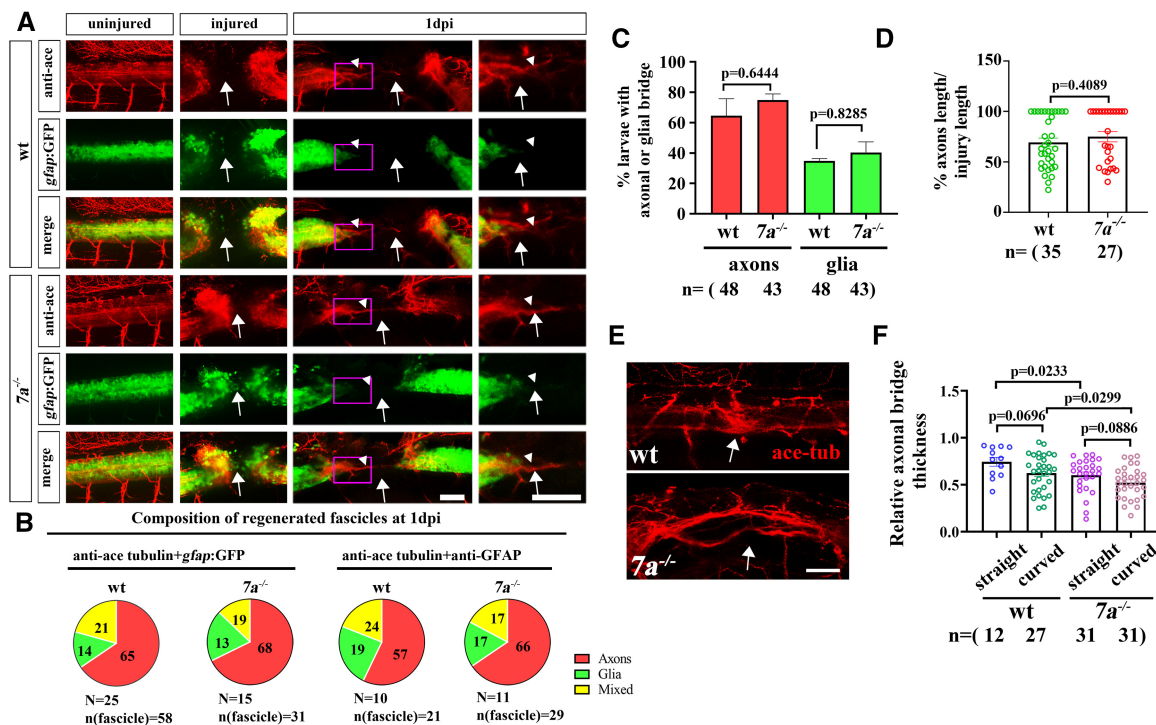


Figure EV2. Axonal regeneration in *rassf7a* mutants after SCI.

- A Representative confocal images showing the regrowth of axons (anti-acetylated Tubulin) and astroglia-like processes (*gfap::GFP*) at 1 dpi. These images show examples of axonal-only fascicles (arrowheads). Arrows indicate injury sites. High magnification images of boxed areas are shown on the right.
- B Quantification of fascicle composition at 1 dpi of wild-type and mutant larvae. The glial processes were visualized with either GFP transgene or GFAP antibody staining.
- C Bar graph showing the percentages of wild-type and *rassf7a* mutant larvae with axonal or glial processes at 1 dpi.
- D Relative axonal bridge length of wild-type and *rassf7a* mutants at 1 dpi.
- E Representative images showing axonal bridges at 5 dpi in wild-type and *rassf7a* mutants visualized with anti-acetylated Tubulin antibody.
- F Dot plots showing relative axonal bridge thickness at the lesion sites of wild-type or mutant larvae at 5 dpi in different groups as indicated.

Data information: *P* values for a Fisher's Exact test (C), unpaired Mann–Whitney test (D) and unpaired Student's *t*-test (F) are indicated. Data are shown as mean \pm S.E.M. Each data point represents an individual fish. Scale bars: 50 μ m in (A, E).

Figure EV3. Neuronal differentiation defects in *rassf7a* mutants after SCI.

Individual channels of Fig 3A showing the localization of BrdU⁺ cells (red) near the lesion sites in wild-type and *rassf7a* mutants carrying different transgenes. Arrows represent lesion sites. Scale bars: 20 μ m.

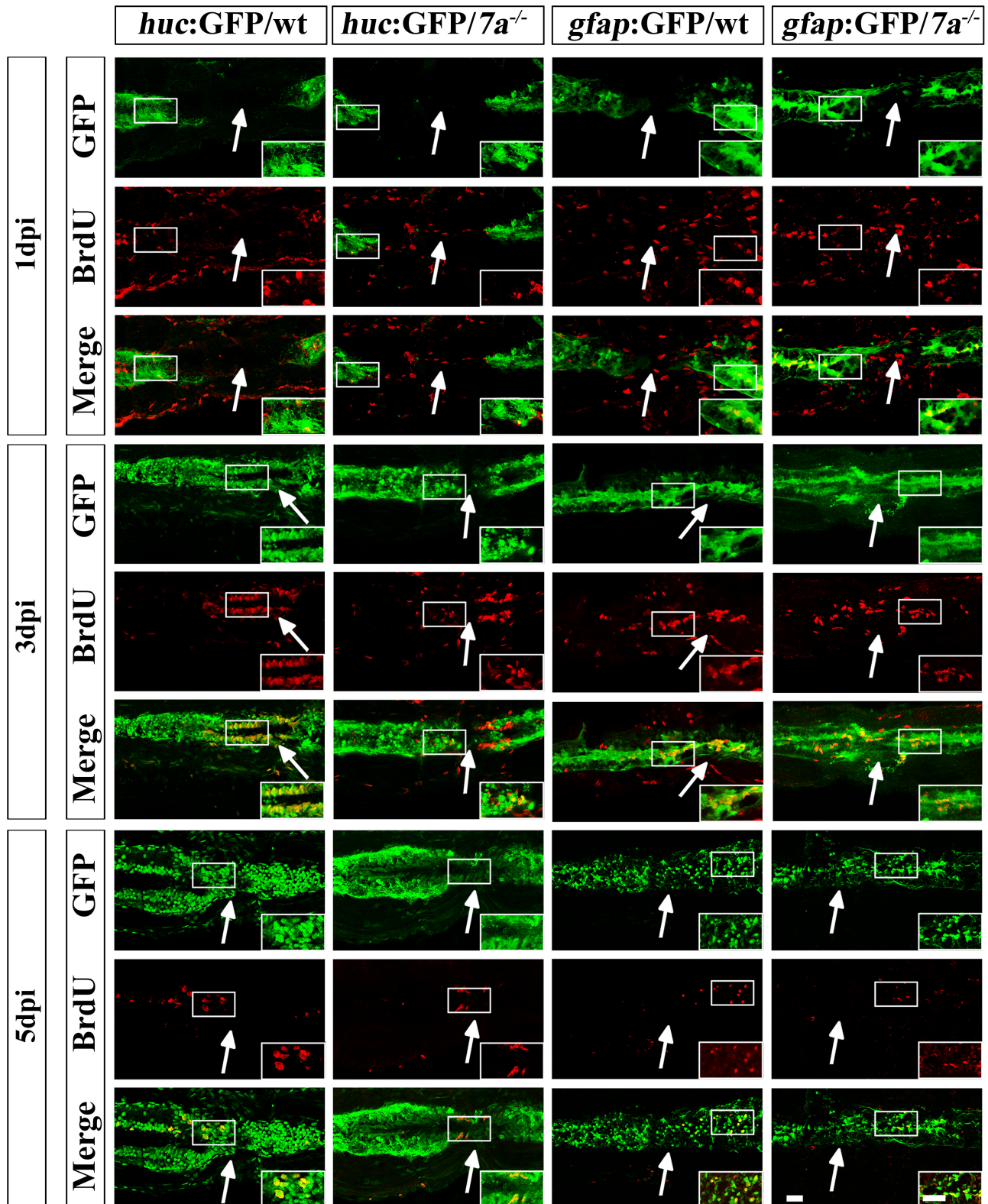


Figure EV3.

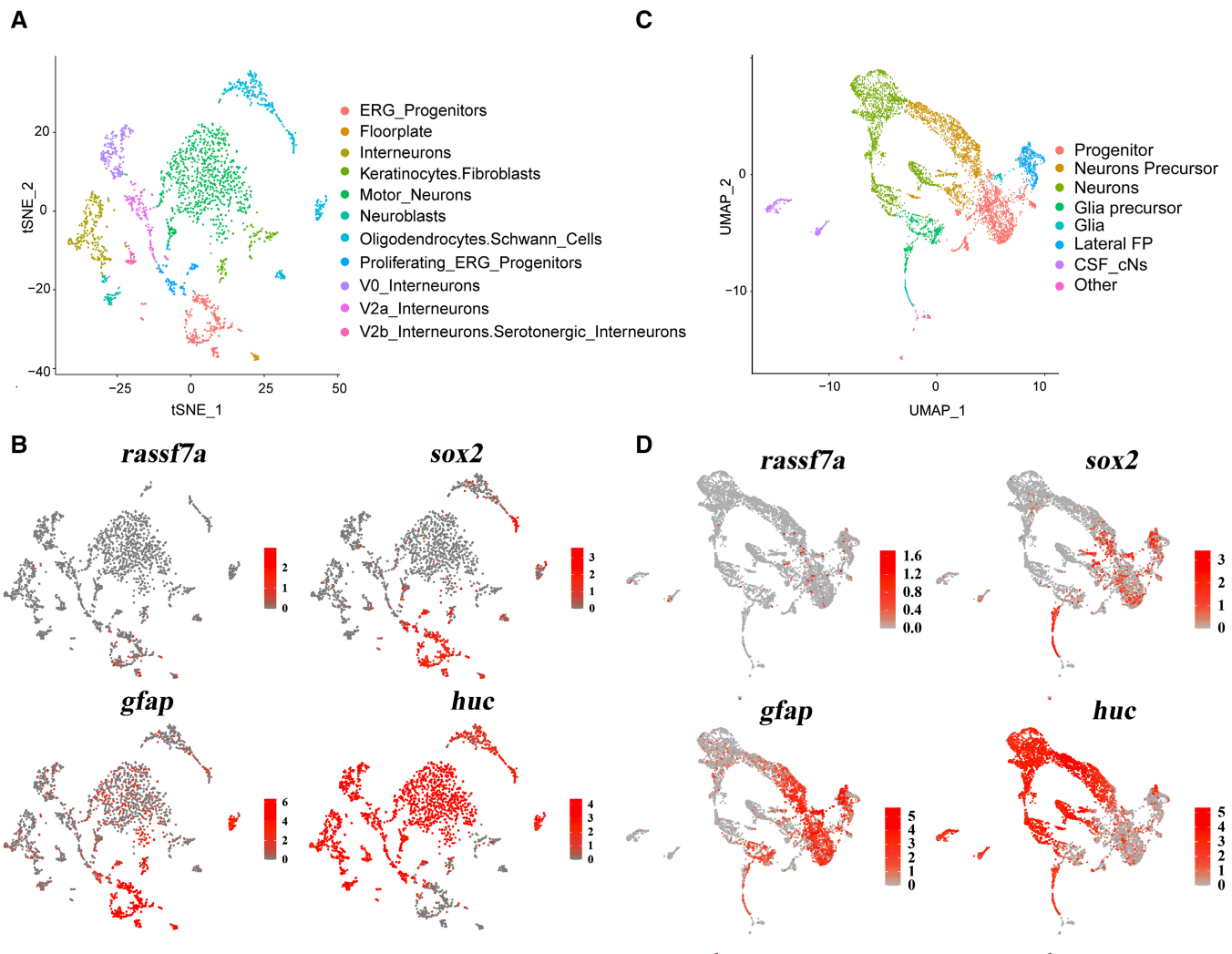


Figure EV4. Expression of *rassf7a* is enriched in the neural progenitor cells.

A A t-distributed Stochastic Neighbor Embedding (tSNE) plot of scRNA-seq dataset (Accession number: SAMEA8658904) from 4 dpf Tg(*her4.3:GFP*) zebrafish larvae.
 B Gene expression patterns of *rassf7a*, *sox2*, *gfap* and *huc* on plot from (A). Color codes indicate normalized expression levels from low (gray) to high (red).
 C Unsupervised UMAP of integrated scRNA-seq dataset (Accession number: GSE173350) from *olig2:EGFP* spinal cord cells obtained from 24 hpf Tg(*olig2:EGFP*) embryos.
 D Gene expression patterns projected onto UMAP plot (from (C)) of *rassf7a*, *sox2*, *gfap* and *huc*.

Figure EV5. Abnormal mitotic spindle rotation of NPCs in *rassf7a* morphants.

A Sequences of time-lapse photographs to illustrate mitotic rotations of a single neural progenitor cell in control or *rassf7a* morphants expressing Sox2⁺-GFP transgene. Anterior is to the left, dorsal is to the up.
 B, C Statistical analysis of angles of mitotic spindle rotation in control or *rassf7a* morphants.
 D History plots of mitotic spindle orientation in control or *rassf7a* morphants at different time points. Green dashed line indicated 45° spindle rotation.
 E Bar graph showing the time of cell division in control or *rassf7a* morphants.

Data information: *P* values for unpaired Mann–Whitney test (B) and unpaired Student's *t*-test (E) are indicated. Data are shown as mean ± S.E.M. Each data point represents a dividing cell. Scale bars: 5 μm in (A).

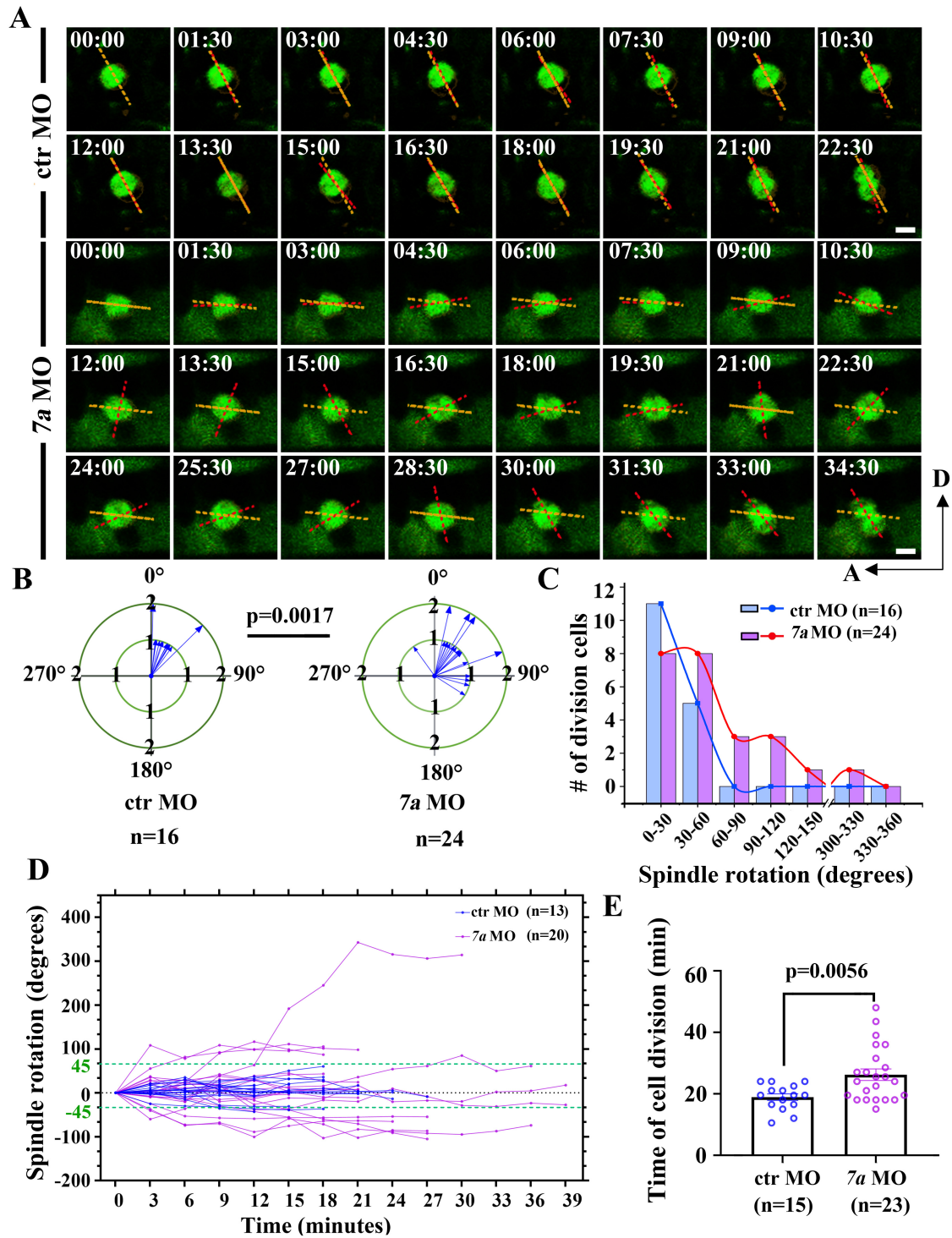


Figure EV5.